Piezoresistive Torque Magnetometry at Low Temperature

Christian Lupien
Center for the Physics of Materials
Department of Physics, McGill University
Montréal, Québec, Canada

A Thesis submitted to the
Faculty of Graduate Studies and Research
in partial fulfillment of the requirements for the degree of
Master of Science

Je dédie cette thèse à Nancy et à ma famille.

CONTENTS

FIGURES AND TABLES

FIGURES

TABLES

RÉSUMÉ

Nous avons utilisé un nouveau type de magnétomètre à moment de force: un cantilever piézorésistif. Il transforme la force appliquée à son extrémité en un changement de sa résistance. Nous présentons la première utilisation de ce dispositif à des températures inférieures à 1 K. Nous avons observé un comportement hystérétique de la résistance sous un faible champ magnétique (inférieur à 10 mT) dans cet interval de température. Sous un champ plus élevé, il a une magnétorésistance qui varie doucement ce qui nous a permis de mesurer l'effet de de Haas-van Alphen (dHvA) de deux supraconducteurs: κ-(BEDT-TTF)$_2$Cu(NCS)$_2$ et Sr_2RuO_4. Ces mesures démontrent qu'un grand courant d'excitation peut-être utilisé si l'échantillon est bien thermalisé mais que l'interaction de moment de force (IMF) peut modifier le signal. L'IMF peut être réduit en utilisant de la rétroaction. Nous présentons aussi des mesures, au-dessus de 75 K, de H_{c1} de $YBa_2Cu_3O_{6.9}$ obtenues en modulant le champ et en mesurant le signal du moment de force à une harmonique de la fréquence de modulation.

ABSTRACT

We have used a new type of torque magnetometer: a piezoresistive cantilever. It detects the force and torque applied to the end of the cantilever beam by changes in its resistance. We report the first use of this device at temperatures below 1 K. We observed a hysteretic behavior of the resistance at low magnetic field (less than 10 mT) in that temperature range. At higher field it has a smoothly varying magnetoresistance which permitted us to measure the de Haas-van Alphen (dHvA) effect in two superconductors: κ-(BEDT-TTF)$_2$Cu(NCS)$_2$ and Sr_2RuO_4. These measurements demonstrated that a large excitation current can be used if the sample is well thermalized but that torque interactions (TI) can affect the signal. TI can be reduced by the use of feedback. We also present measurements above 75 K of H_{c1} of $YBa_2Cu_3O_{6.9}$ obtained by modulating the field and measuring the torque signal at an harmonic of the modulation frequency.

ACKNOWLEDGMENTS

Je veux tout d'abord remercier L. Taillefer, mon directeur de thèse, pour son aide dans la préparation de cette thèse. Il était toujours prêt à répondre à mes questions et à suggérer de nouvelle expérience.

I want to thank B. Ellman from whom I learned a lot about physics and other things for is help on the low temperature techniques, his always entertaining stories, and his help on the data analysis.

Je veux remercier R. Gagnon pour son aide lors de la réparation et de l'utilisation du dipper. Je le remercie aussi pour les crystaux de $YBa_2Cu_3O_{6.9}$ qu'il a mis a ma disposition.

I also want to thank P. Grütter for is advice and intersting discussions about scanning force microscope, cantilevers.

Of course I need to mention the invaluable help of M. Chiao and B. Lussier, which both worked in the same lab as I. They were the one using the fridge.

Thanks to all the people of the machine shop for their assistance in machining different pieces of equipments such as sample mounts.

I would also like to thank all my friends at the physics department. Their presence is essential to forget the lows of experimental physics and to enjoy the highs. They even help to forget completely about physics by organizing activities with no relation to physics, like parties and movies.

The funding organizations also deserve special thanks, without them none of the fun we have working in physics would be possible. Thanks to Conseil de recherche en sciences naturelles et génie, Fonds pour la formation de chercheurs et l'aide à la recherche, the Centre for the Physics of Materials and the Canadian Institute for Advanced Research for their generous contributions to my financial well-being.

1

INTRODUCTION

Torque magnetometers have been used for a long time. They are part of the standard tools to measure magnetization. The others being the Faraday balance (a close cousin to the torque magnetometer, this one using the force instead of the torque), the vibrating sample magnetometer (VSM), the AC susceptometer and the superconducting quantum interference device (SQUID) magnetometer. This last one is the newest and most sensitive at low field.

Since the advent of the scanning probe microscopes (SPM) such as the scanning force microscope (SFM) and the magnetic force microscope (MFM), many new tools to measure small forces have been developed. These are very small and sensitive. They are often microfabricated out of silicon using the same modern techniques used in the semiconducting industry. Some of these devices include their own detection mechanism, making them simple to use and compact. Some of these small devices are not restricted to be used as a scanning probe. For example they can be used as magnetometers by attaching a sample to them, and placing them in a magnetic field.

In this thesis we describe such a new tool. It is a piezoresistive cantilever [1]. It measures forces or torques by changes in its resistance. Since it is very small and sensitive it can measure very small samples, with masses less than 1 μg, and because it is a torque technique its sensitivity increases with field. At a field of 1 Tesla it is more sensitive than commercial SQUIDs by three orders of magnitude [2, 3].

This piezoresistive cantilever was created in 1990 for SFM[1]. In 1995 it was used as a torque magnetometer to study the anisotropy of some high-T_c superconducting compound [3]. This experiment was done above liquid helium temperature (4.2 K). A

low temperature MFM was also constructed using these cantilevers and worked down to 6 K [4].

In this thesis we report the first use of this device below 1 K. We were interested in using such a simple device at low temperatures to make magnetization measurements but since it is a resistive, therefore dissipative device, it was not obvious whether it was going to be a usable tool at such low temperatures. We tested it using the de Haas-van Alphen (dHvA) effect, which is a probe of the Fermi surface, on an organic superconductor κ-(BEDT-TTF)$_2$Cu(NCS)$_2$ [5] and on a newly discovered superconductor Sr_2RuO_4 [6] for which the dHvA effect and angle-resolved photoemission spectroscopy (ARPES) yield different Fermi surfaces [7]. This last compound is isostructural to $La_{2-x}Sr_xCuO_4$, which is a high-T_c superconductor. It is an interesting compound because some experiments impossible in the high-T_c, such as the dHvA effect, can be performed on this material and compared to other techniques, such as ARPES, which have been used extensively on the high-T_c. This tests the applicability and the results obtained from those techniques.

We have also explored another use of the piezoresistive cantilever under different conditions. The dHvA effect required high magnetic fields and low temperature so we tried a measurement at low field (less than 40 mT) and higher temperature (5-100 K). We used a modulation technique to measure the lower critical field of a high temperature superconductor, $YBa_2Cu_3O_{6.9}$.

2

CANTILEVERS

The device used in this thesis is a new kind of cantilever. Cantilever are small beams which have one end fixed. On the other end a force is applied which bends the cantilever. To detect this small deviation many methods can be used. A common method in atomic force microscopy, where small cantilevers are used, is laser interferometry. In this technique a laser beam is aimed, with the help of an optical fiber, at the tip of the cantilever. The fibers also serve as a receiver of the reflected light. The incident and reflected beams are then made to interfere and a fringe detector is used to measure the position. This technique is quite sensitive and can measure displacements as small as 0.01 Å [8].

Another technique is to use capacitance [9]. Here the cantilever is either made bigger or a plate is added to the tip. Another plate is brought very close to the first one. A parallel plate capacitor is then obtained. This type of capacitor has a capacitance which depends inversely on plate separation. Hence with very close plates a sensitivity of 0.02 Å can be achieved [8].

These two techniques both have advantages and disadvantages. The laser technique is quite sensitive, but it requires an optical fiber. This fiber needs to stay aimed at the cantilever. In a low temperature cryostat, during cool down, everything can shift a little because of thermal contraction. Therefore to use this technique a motor is needed to compensate any displacements. The capacitance technique is often used at low temperature because it is dissipationless. A large excitation can be used without warming up the cantilever. But the capacitance is often very small, and care must be taken to avoid parasitic capacitance which can be orders of magnitude bigger.

Used as magnetometers, cantilevers are especially suited for angular dependence. For example, with superconductors, the torque signal when the field changes orientation contains both a reversible and an irreversible part. Assuming a certain model for the reversible torque, many parameters of the materials can be extracted: upper critical field, penetration length and the effective-mass anisotropy [10]. From the irreversible torque other parameters such as critical current and activation energies [11, 12, 13] are obtained. In the above references, all authors used capacitive torque magnetometers which were not microfabricated cantilevers, but similar results can be obtained with the later. The advantage over other techniques is that torque magnetometry is a bulk measurement and does not need contacts on the sample. It is usually a compact system which can be used at different temperatures and can easily be rotated. It also measures directly the perpendicular component of the magnetization, hence it is a sensitive probe to magnetic anisotropy.

Now because of some of the needs of atomic force microscopy many new types of cantilevers are being developed. Some of them have the detection mechanism included in the cantilever itself. One such device is the piezoresistive cantilever.

2.1 *Piezoresistive cantilever*

As the name suggests this device detects the deviation by changes in its resistance. Fig. (2.1) shows a microphotography of the device and fig. (2.2) shows its dimensions. It is microfabricated out of silicon [1, 14]. They were invented by Tortonese *et al.* [1] and can be obtained from Park Scientific Instruments (PSI). The two small legs are the cantilever beams. This geometry makes it preferentially bend up and down (along z) and prevents left-right (y) motion (see fig. (2.3)). On the flat end a tip can be added to do force microscopy, or a sample can be placed. Of the 4 μm thickness only the first μm is heavily doped with Boron ($\approx 10^{19}$ ions/cm^3), making it conductive (p-type). This conductive layer is the detection mechanism. When the cantilever bends – lets assume down – then it gets deformed. The bottom layer gets compressed and the top layer gets stretched. But since only the top layer is

Figure 2.1: Microphotography of a piezoresistive cantilever.

conductive only the stress on it will change the resistance. Now this material has a high sensitivity to stress. This is because it is close to a metal-insulator transition [15]. This can be viewed as follows: an impurity has a wavefunction with a large spatial extent, but at low densities the Ψ of different impurities do not overlap and we have an insulator at low temperature. As the density is increased past the critical density n_c, the wavefunctions overlap enough to have a conductor at low temperature. For boron-doped silicon $n_c = 4.06 \times 10^{18}$ cm^{-3}[16]. Close to this concentration many parameters, like resistivity, are very sensitive to density. Small changes in density due to an applied stress are enough to modify these. Even the critical density is pressure dependent [15]. Actually for the cantilevers we use, a change in resistance of one part per million (ppm) corresponds to a motion of 0.4 Å as given by PSI.

These cantilevers have been used in both room temperature and low temperature (6 and 77 K) atomic force microscope with a resolution of 0.1 Å [4, 17]. They have also been used as torque magnetometers by Rossel *et al.* [2, 3], who used the angular dependence of the torque to measure the effective mass anisotropy of superconductors, at about 100 K.

The advantages of a microfabricated cantilever is that its characteristics can be obtained reproducibly. A rough calibration of one cantilever should apply to another

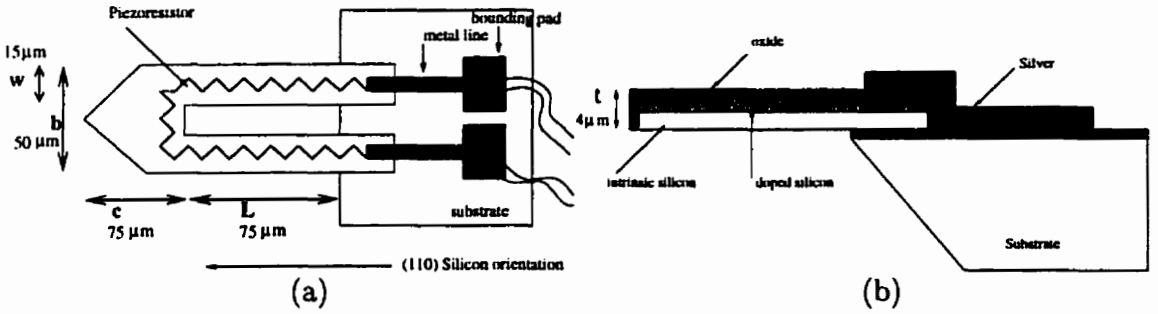

Figure 2.2: Description of the piezoresistive cantilever. (a) is the top view showing the dimensions and (b) is a side view showing the construction profile.

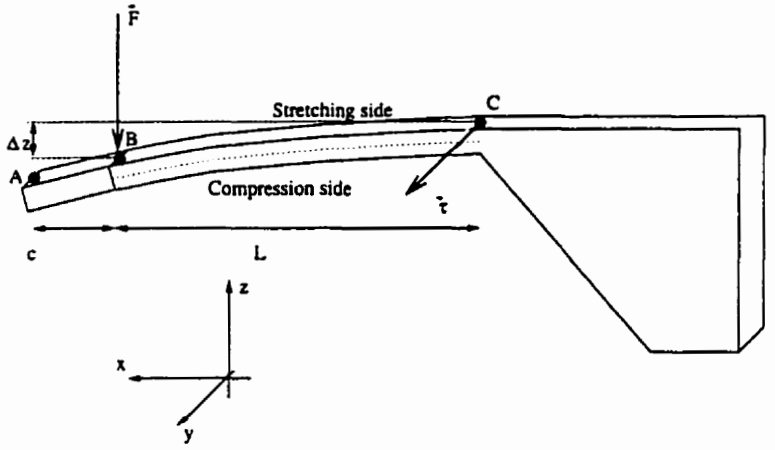

Figure 2.3: Force diagram on cantilever. The flexible section is between points B and C. Samples are attached between A and B.

one. Their mechanical characteristics are those of good quality single crystal of silicon which is both strong and light. This permits the construction of cantilevers with high quality factor and high resonance frequency, required for modern atomic force microscopes using modulation techniques.

2.2 Force and torque

We are concerned with magnetic force and magnetic torque. For a sample of magnetic moment $\vec{\mathcal{M}}$ in an applied magnetic field $\vec{H}$ the force $\vec{F}$ and torque $\vec{\tau}$ are:

$$\vec{F} = \mu_o \vec{\nabla}(\vec{\mathcal{M}} \cdot \vec{H}) = \mu_o(\vec{\mathcal{M}} \cdot \vec{\nabla})\vec{H} \tag{2.1}$$

$$\vec{\tau} = \mu_o \vec{\mathcal{M}} \times \vec{H} \tag{2.2}$$

These are very general results of magnetostatics. They can also be derived from thermodynamics. This is less general since some systems do not have a well-defined thermodynamic magnetic energy. For example iron shows hysteresis: it can have different magnetizations at a particular field.

In the next chapters we use statistical mechanics and thermodynamics to obtain some results. Therefore we now present a precise thermodynamic definition of a system with magnetic energy. We will start from a standard definition of magnetic energy and define more useful free energies. When discussing thermodynamics, we always need to be careful about the distinction between different free energies and we will clarify the situation.

2.2.1 *Precise thermodynamic definition*

Usually the thermodynamic work done on a magnetic system (W_m) is given by [18, 19]

$$W_m = \int_{\text{Volume}} \int^{\vec{B}} \left(\vec{H} \cdot d\vec{B}\right) d^3x, \tag{2.3}$$

where $\vec{B}$ is the magnetic field and $\vec{H} = \frac{1}{\mu_o}\vec{B} - \vec{M}$ in the MKS system. $\vec{M}$ is the magnetization [18]. Notice that this work includes the energy needed to setup a field in vacuum.

We can write the change in internal energy (U) for an infinitesimal process as

$$dU = dQ + dW = TdS + \int_{\text{Volume}} \left(\vec{H} \cdot d\vec{B}\right) d^3x - \vec{F} \cdot d\vec{x} - \tau d\theta. \tag{2.4}$$

where we have included in the work (dW) the magnetic work described above, the mechanical work done in displacing the sample by $d\vec{x}$ under a force $\vec{F}$, the $-\vec{F} \cdot d\vec{x}$ term, and the mechanical work done in rotating the sample by $d\theta$ with a torque τ (along the rotation axis of θ), the $-\tau d\theta$ term. Also Q is the heat going into the system, T is the temperature and S the entropy. We have used the fact that for an infinitesimal reversible process $dQ = TdS$ [20]. Therefore the change in internal energy is given by the heat transfer, the work done by the magnetic field, the displacement and the rotation. Also this infinitesimal representation tells us which variables are independent for this free energy. Here they are S, $\vec{x}$, θ and $\vec{B}$. For example this means that if

a process keeps all these independent variables constant then $U_{initial} = U_{final}$. Also, from eqn. (2.4) we can write $\vec{F} = (\vec{\nabla}_{\vec{x}} U)_{S,\vec{B},\theta}$, $T = (\partial U/\partial S)_{\vec{B},\vec{x},\theta}$, etc. Therefore T, $\vec{H}$, $\vec{F}$ and θ are all functions of the independent variables. These functions can be used to replace an independent variable by a dependent one. For example U can be expressed in terms of T instead of S. But this substitution does not change the infinitesimal representation (eqn. (2.4)) which says that U is obtained for a system in which S is controlled.

We are often interested in systems in contact with a large heat reservoir which defines their temperature. In this case it is no longer the entropy which specifies the system but the temperature. Therefore we must perform a Legendre transformation to obtain a new free energy. We let $\mathcal{F} = U - TS$ and obtain that for an infinitesimal reversible process that $d\mathcal{F} = -SdT + dW$, where dW is the same as in eqn. (2.4). Hence for $\mathcal{F}$, the temperature (T) is now an independent variable. Since we are also mostly interested in systems defined with the applied field $\vec{H}$ instead of by $\vec{B}$ we perform another Legendre transformation by defining a new free energy $\mathcal{G} = \mathcal{F} - \int_{\text{Volume}} \vec{H} \cdot \vec{B} d^3x$ and we obtain for the infinitesimal reversible process:

$$d\mathcal{G} = -SdT - \int_{\text{Volume}} \left(\vec{B} \cdot d\vec{H}\right) d^3x - \vec{F} \cdot d\vec{x} - \tau d\theta, \tag{2.5}$$

where the independent variables are found to be T, $\vec{H}$, $\vec{x}$ and θ. This is equivalent to the transformation done on a hydrostatic system to obtain the Gibbs free energy.

Up to now the magnetic energy includes the vacuum energy. Since that energy is there even without the sample present we can remove it to obtain a free energy corresponding only to the effect of the material. So we write $\mathcal{G}' = \mathcal{G} + \int_{\text{Volume}} \mu_o \left(\vec{H}_a \cdot d\vec{H}_a\right) d^3x$ but it can be shown that (see [19]):

$$\int_{\text{Volume}} \left(\vec{B} \cdot d\vec{H}\right) d^3x - \int_{\text{Volume}} \mu_o \left(\vec{H}_a \cdot d\vec{H}_a\right) d^3x = \int_{\text{Volume}} \mu_o \left(\vec{M} \cdot d\vec{H}_a\right) d^3x \tag{2.6}$$

so that

$$d\mathcal{G}' = -SdT - \int_{\text{Volume}} \mu_o \left(\vec{M} \cdot d\vec{H}_a\right) d^3x - \vec{F} \cdot d\vec{x} - \tau d\theta, \tag{2.7}$$

where $\vec{H}_a$ is the applied field with the sample replaced by vacuum. This can be different from $\vec{H}$ because $\vec{H}$ gets modified by the demagnetizing field of the sample.

From this infinitesimal representation we find that $\vec{M} = \frac{1}{\mu_o}(\vec{\nabla}_{\vec{H}_a} g')_{T,\vec{x},\theta}$[1] where g' is the free energy density of $\mathcal{G}'$, *i.e.* without the volume integral, and $\vec{\nabla}_{\vec{H}_a}$ is the gradient with respect to $\vec{H}_A$ taken at constant T, $\vec{x}$ and θ. Similarly $\vec{F} = -(\vec{\nabla}_{\vec{x}} \mathcal{G}')_{T,\vec{H}_a,\theta}$ and $\tau = -(\partial \mathcal{G}'/\partial\theta)_{T,\vec{H}_a,\vec{x}}$. Assuming a uniform magnetic field we also obtain the magnetic moment: $\vec{\mathcal{M}} = \frac{1}{\mu_o}(\vec{\nabla}_{\vec{H}_a} G')_{T,\vec{x},\theta}$. With a similar assumption eqn. (2.1) and eqn. (2.2) are derived.

$\mathcal{G}'$ is the magnetic free energy most frequently used. It corresponds to systems with a specified temperature and external magnetic field. If a partition function (Z) of a canonical ensemble is developed with a defined external field as a parameter then $\mathcal{G}' = k_B T \ln Z$ where $k_B = 1.38 \times 10^{-23}$J/K is Boltzmann's constant. This is similar to a hydrostatic system where $F = k_B T \ln Z$, F being the Helmholtz free, and the partition function has the volume as a parameter [20, 21, 22].

From now on the subscript a and the prime on $\mathcal{G}'$ will be dropped. You should note that the literature has no convention for the free energy of magnetic systems similar to that for hydrostatics. Often F is employed where $\mathcal{G}$, in my convention, should have been used.

2.2.2 *Theoretical spring constant and sensitivity*

When a sample is placed in a uniform field no force is exerted on it. But because of shape (demagnetization factors) or anisotropy in the susceptibility a torque can still be exerted on the sample by the field. Fig. (2.3) shows the force diagram. If we rigidly attach the sample to the end of the cantilever (between A and B) the torque gets transfered to the pivot point (C) of the cantilever. Therefore the torque on the sample translates into a force on the tip of the cantilever.

$$F_z = \frac{\tau_y}{L} \tag{2.8}$$

where L is the distance between the pivot (C) and the point at which the force is to be measured (point B). $L \approx 75$ μm for the cantilever we used. We use point B

[1] This shows one limit of the thermodynamic approach. It will always give magnetization with $\vec{\nabla}_{\vec{H}_a} \times \vec{M} = 0$. Generally $\vec{M}$ could have a non zero curl but those systems cannot be described by thermodynamics and do not occur in this thesis.

because that is the end of the bending part of the cantilever and where the spring constant is most easily calculated.

We will now proceed to obtain some rough estimates of spring constants, angular deviations and sensitivity. We should mention that the elastic deformation actually depends on the stress which is applied. This stress has different distributions depending on whether it is a torque or a force which is applied on the tip. It even depends on the actual point on the tip where the force is applied. In what follows we do not consider these differences since we are only interested in estimates.

We obtain the displacement Δz from the force by using the elastic constant (K) of the beam:

$$\Delta z = \frac{F_z}{K} \tag{2.9}$$

where K=20 N/m for the cantilevers we used as given by PSI. This can be estimated from the formula of elastic theory[23, 24, 8] in which E is the Young Modulus of the material, I is the moment of inertia of the section, and L is the length of the beam:

$$K = \frac{3EI}{L^3}. \tag{2.10}$$

We have $I = wt^3/12$ for a rectangular section of width w and thickness t, for a bending along the thickness direction. $I = \pi r^4/4$ for a circular section of radius r. For the cantilevers we used, we had two parallel rectangular beams with $L = 75$ μm, $w = 15$ μm, $t = 4$ μm and for silicon $E = 11 \times 10^{10}$ N/m^2. Since the spring constants of two parallel springs add:

$$K = \frac{Ewt^3}{2L^3} = 125 \text{ N/m}. \tag{2.11}$$

This is the spring constant for the force and displacement measured at B in fig. (2.3). The spring constant given by the manufacturer is for a force and displacement measured at point A. To obtain the effective spring constant there, we use that along the bending part of the beam (from B to C)

$$\Delta z(x) = \frac{3F_z}{6KL^3}\left(3Lx^2 - x^3\right), \tag{2.12}$$

where $x = 0$ at point C. This is obtained from the elastic theory of beams [23, 25]. Of course this gives that $F_Z/\Delta z(L) = K$. We want to know $K_A = F_Z/\Delta z(L+c)$. Since from A to B the beam is straight and at the angle (θ) of point B we can write for small displacement,

$$\tan(\theta) \approx \theta = \frac{d\Delta z}{dx} = \frac{3F_z}{4KL^3}\left(Lx - 2x^2\right). \tag{2.13}$$

So we obtain that

$$\Delta z(L+c) = \Delta z(L) + c\theta(L) = \frac{F_z}{K} + c\frac{3F_z}{2KL} \tag{2.14}$$

which gives $K_A = K(1+3c/2L) = 125(1+3/2) = 50$ N/m since both L and c are 75 μm. This is close to the manufacturer number of 20 N/m since the spring constant is very sensitive on thickness. This factor of 2.5 can be obtained if instead of 4 μm the thickness was 3 μm. We have also assumed that the section from A to B does not bend, which is not accurate and as stated above we are only doing an estimate. If we took the force to act at point A instead of B and used the real formulas and the 4 μm thickness we would obtain a better result.

We can also obtain the resonance frequency f

$$f = \frac{\omega}{2\pi} = \frac{1}{2\pi}\sqrt{\frac{K}{m_{eff}}} \tag{2.15}$$

where $m_{eff} = 0.243m_d + m$ for a uniformly distributed mass along the beam of m_d and an additional mass at the end of the beam of m. Using a silicon mass density of 2.33 g/cm^3 which leads to $m_d = 0.021$ μg and $m = 0.026$ μg and $K = 20$ N/m we get $f = 127$ kHz (the manufacturer gives 120 kHz), while if we use the mass of a typical sample, $m = 25$ μg, we get 4.5 kHz.

Calculating the piezoresistance effect in the cantilever is more complicated since it depends on the exact doping profile of the cantilever [17]. If it is uniformly doped over the full thickness, then $\Delta R/R_o\Delta z = 0$, where ΔR is the change in resistance of the cantilever and R_o is its resistance with no applied stress. Of course this would be useless. Our cantilevers are doped only over the first quarter of the thickness and this

gives a non-zero effect. The manufacturer reports a sensitivity of $\Delta R/R_o\Delta z = 0.4$ ppm/Å for our piezoresistive cantilevers at room temperature.

The appendix lists the conversion factors between vertical displacement, force, torque, angular motion, resistance change and relative resistance change. These are obtained using the numbers given by the manufacturer (PSI) and some of the relations developed in this section.

2.3 *Cantilever characteristics*

For the measurement of magnetization at different temperatures we are interested in the behavior of many of the above constants as a function of temperature. Rossel *et al.* measured the resonance frequency of a similar cantilever from room temperature down to 10 K. Since over that range it changed only by 0.4% we know that the spring constant changes by less than 1%. Below 100 K it is essentially constant. From 100 K to room temperature it falls linearly. Using the technique described in chapter 5 we measured that the piezoresistive coefficient actually increases a little when you cool down as seen on fig. (2.4), in agreement with measurements on doped silicon [26] and by C. W. Yuan who reported an increase of sensitivity of 2.4 between room temperature and 6 K [4] using similar piezoresistive cantilevers. Fig. (2.4) was obtained by looking at the magnetization at constant field of a sample of $YBa_2Cu_3O_{6.9}$. The field was small enough, 3 mT, to be in the Meissner state of the superconductor. There the sample repulses all field and the magnetization is $\vec{M} = -\vec{H}$. From the second harmonic signal obtained from the technique of chapter 5 we obtain a signal which only depends on the geometry of the sample, if we are far enough below T_c that the magnetic field penetration depth can be assumed small. Under these conditions a change in the signal can only be due to the piezoresistive constant since the geometry and the spring constant do not change.

Another important characteristic is the behavior of the resistance without stress as a function of temperature. If it had no temperature dependence (for any field), then any signal observed under temperature sweeps would be due solely to the sample.

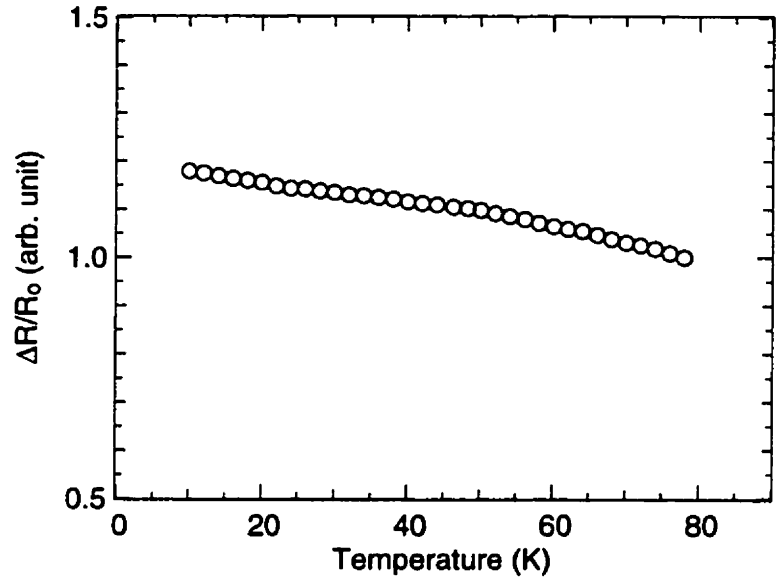

Figure 2.4: Sensitivity of cantilever normalized to 1 at 80 K obtained from the second harmonic signal of a $YBa_2Cu_3O_{6.9}$ sample (see chapter 5).

This is not the case. Fig. (2.5) shows that the resistance is not constant: it varies between 2.2 and 2.6 kΩ. Therefore, with a temperature sweep a simple DC change of resistance is composed of the force signal itself and the temperature dependent resistance. Also any temperature noise will be transformed into resistance noise. This can cause problems especially when the slope is high like around 25 K and 120 K (slope of 4 Ω/K) but it will be small around 60 K and 240 K (slope is 0). Below 1 K the slope is about 125 Ω/K. The fact that the resistance stays to within 10% of 2.4 kΩ makes the measuring electronics a lot simpler: no change of scale is necessary.

A last point to note is the dependence of the resistance on magnetic field, *i.e.* the magnetoresistance of the piezoresistive cantilever. This is shown in fig. (2.6). It is measured at 70 mK in a dilution refrigerator (see chapter 4). While being a small change, this might still be bigger than small DC signals. Therefore these cantilevers are not the best tool for field sweeps (or temperature sweeps of linear signals). But it can detect abrupt and oscillatory changes very easily, or of course signals large compared with these variations in resistance.

Fig. (2.7) shows a problem that occurs with those cantilevers at low temperature, and very small fields. They show a large and hysteretic change in resistance. This

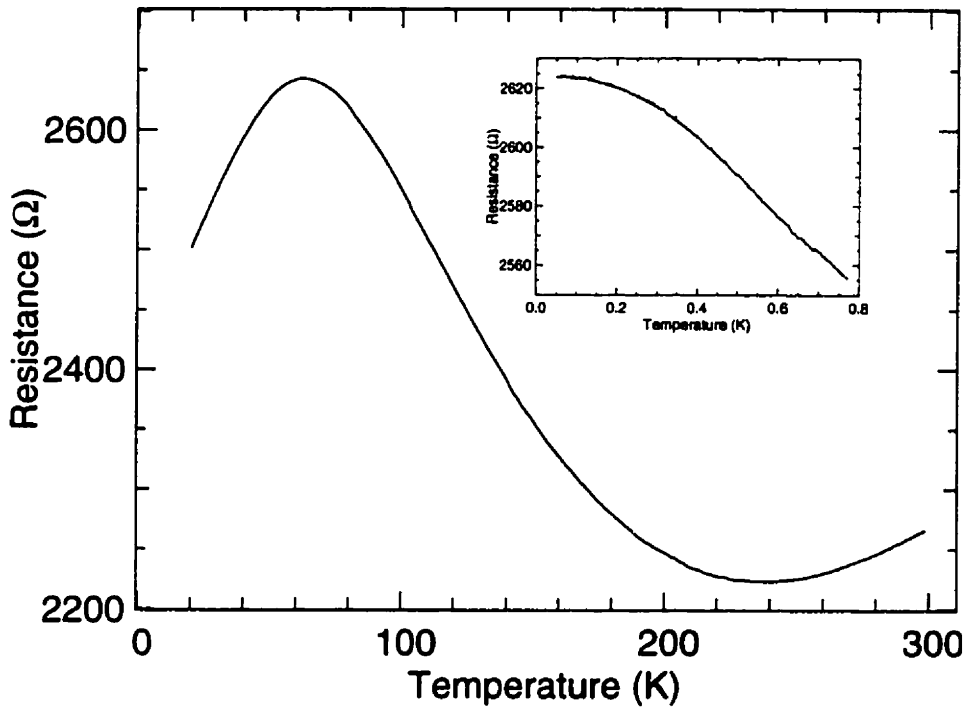

Figure 2.5: Temperature dependence of the resistance of the cantilever. The inset shows the behavior below 1K. Note that the two graphs were not obtain with the same cantilever, the insert as been renormalized to some incomplete data obtain for the same piezo as in the main graph. The flattening of the curve below 0.3 K is caused by self-heating (0.04 μA excitation).

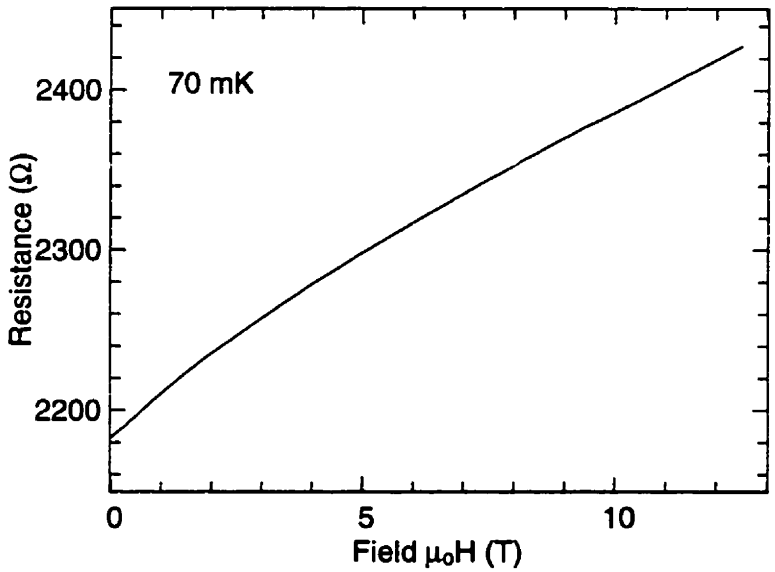

Figure 2.6: Magnetoresistance of piezoresistive cantilever measured at 70 mK.

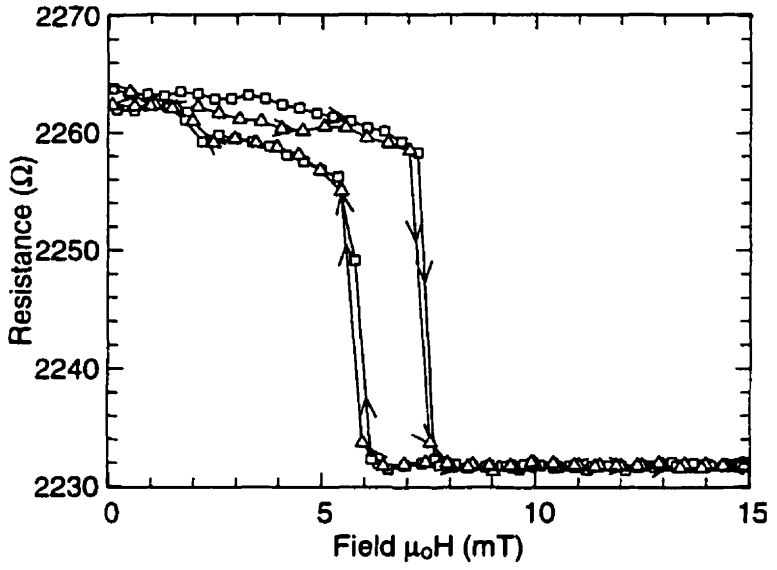

Figure 2.7: Low field hysteresis behavior of cantilever at 800 mK. The graph shows two sets of data (triangles and squares). The arrows show the direction of field sweep.

hysteresis repeats really well and the bumps are not due to noise. As the temperature is raised this behavior occurs over a smaller range of field and disappears at liquid helium temperature 4.2 K. This large effect prevents the measurement of signals at fields below 15 mT (below 1K). We do not understand this behavior but we think it can be due to a weak localization problem where the resistance is sensitive to the actual position of the impurities.

2.4 *Noise sources*

Many noise sources can limit the sensitivity of the measurement. Some of these can be improved. For example inductive pick up noise can be improved by using twisted pair of wires. Capacitive pickup by using shielded wires. But some sources are intrinsic limits to the measurement. One of these is the Johnson noise. This is the white noise (independent of frequency) of every resistance. It is given by

$$V_{RMS}^{noise} = \sqrt{4k_B T R \Delta f} \tag{2.16}$$

where $k_B = 1.38 \times 10^{-23}$ J/K is Boltzman's constant, T is the temperature, R is in Ohms and Δf is the bandwidth in Hz. For a 2 kΩ resistor, at room temperature

(300 K) and a bandwidth of 1 Hz this noise is 6 nV_{RMS}, which is 3 ppm of the full scale signal with a 1 μA excitation through R. Of course this can be improved by cooling the resistor to a lower temperature or by using a smaller bandwidth. Since we use the cantilever at low temperature we lower the noise. Using a smaller bandwidth is difficult since it implies you have to wait longer for every data point. Therefore a compromise must be reached between measurement speed and noise. This is the reason for the use of filters of about 1 Hz.

Every resistor also has another noise source called pink noise. This one has $V_{RMS}^{noise} \propto 1/f$. The constant of proportionality is material dependent. It can vary from one resistor to another. But because of the inverse frequency relation, this noise can be minimized by doing measurements at high frequency (0.1-10 kHz).

Of course these noise sources are independent of the excitation current through the resistor so the signal to noise ratio can be improved with a higher excitation current. This also decreases the shot noise of the current. This noise is caused by the discreteness of the charge carriers, which yields a count noise given by Poisson's statistics and is given by:

$$I_{RMS}^{noise} = \sqrt{2qI\Delta f} \tag{2.17}$$

where I is the RMS current in amperes and $q = 1.6 \times 10^{-19}$ C is the electron charge. For a small excitation current of 1 μA and bandwidth of 1 Hz the noise is .5 pA, which is less than 1 ppm of the full signal. Therefore the shot noise is usually smaller than the Johnson noise for our piezoresistive cantilevers.

A last noise source that affects the resistance measurement directly is the temperature drifts and noise. As was shown above the temperature coefficient of the resistance varies between -4 to +4 Ω/K above 10 K and reaches -120 Ω/K below 1 K. This is not improved by increasing the excitation current. Only good temperature control, better than 1 mK, can limit this problem. Of course this is not a problem at the points where the temperature coefficient is zero. But this particular situation only exists in very small temperature ranges.

The other source of noise is the vibration of the cantilever itself. This can be due

to external vibrations that couple to the cantilever. For example the building and pump vibrations can force the cantilever to vibrate. These sources can be eliminated by a good vibration isolation of the cantilever. This can be achieved with springs, stacks of weakly coupled plates etc. Even with no external excitation, thermal noise makes the cantilever vibrate. This intrinsic vibrational noise of the cantilever is [8]:

$$\left\langle \Delta z^2 \right\rangle = \frac{4k_B T \Delta f}{K} \frac{Q\omega_o^3}{Q^2(\omega_o^2 - \omega^2)^2 + \omega_o^2\omega^2} \tag{2.18}$$

where Q is the quality factor of the cantilever, ω_o the resonance frequency and Δf is the bandwidth centered at ω. If we assume that we are off resonance ($\omega \ll \omega_o$) then

$$\left\langle \Delta z^2 \right\rangle = \frac{4k_B T \Delta f}{KQ\omega_o}. \tag{2.19}$$

With $Q = 10$ and $\omega_o = 2\pi 100$ Hz and $K = 20$ N/m, at room temperature (300 K) and with a bandwidth of 1 Hz we get 0.004 Å_{RMS} of noise. This is very small and has not been reached yet for these devices. The parameters used here are estimates for a cantilever with a large sample on the tip. Both Q and ω_o could be bigger, which would mean a smaller noise. An unloaded cantilever has $\omega_o = 2\pi 120$ kHz and $Q = 315$ at atmospheric pressure and $Q = 16000$ under vacuum.

We achieved a sensitivity of 1 mΩ (about 1 Å or 0.4 ppm) at moderate temperature (10-100 K see chapter 5) and 10 mΩ (10Å or 4 ppm) below 1K. This can be improved by better shielding and higher excitation current. As an atomic force microscope Tortonese *et al.* achieved a resolution of 0.1 Å_{RMS}[17]. Using it as a torque magnetometer it can be more sensitive than a superconducting quantum interference device (SQUID) magnetometer. Zech *et al.* report a sensitivity of 10^{-14} Nm (0.1 Å) which is equivalent to a magnetic moment of 10^{-14} Am^2 at 1T [2]. This is three orders of magnitude better than commercial SQUIDs [3] which have a sensitivity of $10^{-11} - 10^{-12}$ Am^2.

3

SUPERCONDUCTIVITY THEORY

All the samples we used in our experiments were superconductors. Therefore we present here a short introduction to superconductivity and present the characteristic properties that will be used later. We refer the reader to books by Tinkham [27], de Gennes [28] and Parks [29] for a more in depth discussion of superconductivity.

3.1 General

Superconductivity was discovered in 1911 by Heike Kamerlingh Onnes. He found that the resistivity of mercury abruptly dropped to zero below a critical temperature labelled T_c. Following this discovery many other metals were found to exhibit the same behavior. The highest transition temperature for an elemental metal is T_c=9.2 K for Niobium. The second piece in the superconductivity puzzle was found by Meissner and Ochsenfeld in 1933 who noticed that the magnetic field was expelled from the interior of samples ($\vec{B} = 0$) cooled below the superconducting temperature with a magnetic field applied. This is perfect diamagnetism, and is called the Meissner effect. This is not implied by perfect superconductivity. If a conductor is cooled in a field below a temperature where $\sigma = \infty$ it will not expel the field. This also implies the existence of a critical field H_c above which superconductivity is destroyed. There is a surface current which develops to cancel the effect of the field. The field decays smoothly from its value at the surface to zero inside over a length called the penetration length, λ.

Theorists then had the two important characteristics of a superconductor. Various authors put forward different phenomenological models to explain the properties of

superconductors: the London model for the Meissner effect, the two fluid model for the temperature dependence of certain properties, the Pippard model to explain the non-local electrodynamics of superconductors and the Ginzburg-Landau (GL) theory, a general phenomenological theory of phase transitions.

Then in 1957, Bardeen Cooper and Schrieffer (BCS) developed a simple theory [30] that explained well virtually all superconducting properties that were then known. That BCS theory is based on the fact that there is a small attractive potential between electrons. This causes an instability of the electron gas which then leads to the formation of bound electron pairs, called Cooper pairs. The paired electrons have equal but opposite momentum and opposite spins. The attractive potential was assumed to come from interactions of the electron with the lattice. This is simple to understand. When an electron moves through a lattice it attracts the surrounding positive ions. These have a heavy mass compared to the electrons so their response is slower. A certain time after the first electron has passed, there is still a slightly positive charge which can attract another electron. Therefore the two electrons have interacted with the exchange of a phonon, a lattice vibration. Obviously the electrons are separated in both time and space. We usually refer to the average pair separation as the coherence length ξ. For example, $\xi = 16\,000$ Å in pure aluminum and $\xi = 380$ Å in niobium.

Observing that the paired electrons are at the heart of superconductivity, the BCS theory combines the pairs together into a single, macroscopic wave function Ψ_{BCS}:

$$\Psi_{\mathrm{BCS}} = \prod_{\vec{k}} \left(u_{\vec{k}} + v_{\vec{k}} a^{\dagger}_{\vec{k}\uparrow} a_{-\vec{k}\downarrow} \right) |0\rangle \tag{3.1}$$

where $\left|v_{\vec{k}}\right|^2$ is the probability of a pair state $\vec{k}$ being occupied, $\left|u_{\vec{k}}\right|^2$ is the probability of a pair state $\vec{k}$ being unoccupied and the $a^{\dagger}$'s are standard creation operators from second quantization.

Using eqn. (3.1) in an Hamiltonian with a small attractive interaction between electrons, we obtain the excitation spectrum ($E_{\vec{k}}$) in the superconducting state:

$$E_{\vec{k}} = +\sqrt{\varepsilon^2_{\vec{k}} + \left|\Delta_{\vec{k}}\right|^2} \tag{3.2}$$

where $\varepsilon_{\vec{k}}$ is the single quasiparticle energy measured from the Fermi level and $\Delta_{\vec{k}}$ is the energy gap. This energy gap represents the smallest energy required to excite an electron from the ground state. Since the electrons are paired this actually corresponds to the breaking of a pair. The gap is temperature dependent. It goes to zero at T_c but below about 0.4 T_c it is constant and is of the order of $k_B T_c$. Actually with the assumptions of isotropic Fermi surface and of weak isotropic interaction between electrons BCS finds an isotropic gap with a zero temperature value $\Delta(0)/k_B T_c = 1.76$.

These last conditions of isotropicity and of weak coupling were part of the initial BCS *model*. The model can be relaxed by assuming some anisotropy of the Fermi surface, of the coupling and by having a strong coupling. These assumptions lead to similar results, but the ratio $\Delta(0)/k_B T_c$ now depends on the strength of the coupling and the gap can have different amplitudes in different directions.

3.2 Conventional vs unconventional

There are many definitions of unconventional superconductivity. The BCS *model* described in the previous section depends on an electron-phonon mechanism for the formation of Cooper pairs. In contrast to this the BCS *theory* is the general tool to use to produce superconductivity by pairing electrons with some attractive force. We can therefore define unconventional in two ways: superconductors not explained by the BCS *model* and superconductors not explain by the BCS *theory*. The second definition is too restrictive so we define as unconventional a superconductor where the attractive interaction is not due to an electron-phonon mechanism. This can lead to a gap structure which is very anisotropic. The high anisotropy for example can be that the gap disappears in a certain direction. We call that a node.

From the above definition the heavy fermions, the high-T_cs and the organic superconductors are all unconventional. They all have superconducting characteristics which suggest that the coupling is not phonon mediated and also that there are nodes in the gap. They all have an anti-ferromagnetic phase close (or in the case of the heavy-fermion coexisting with) the superconducting phase. This suggests that mag-

netism plays an important role in the superconductivity of the three groups mentioned above. The nature of the coupling mechanism still remains an open question. Also, an active area of research on those materials is to find the positions of the nodes.

3.3 The Meissner state and H_{c1}

We mentioned the existence of a critical field in a previous section. This is understood if we compare the free energies of the superconducting ($\mathcal{G}_S(T,H)$) and normal state ($\mathcal{G}_N(T,H)$) in a magnetic field. The superconducting state will be preferred as long as $\mathcal{G}_S(T,H) = \mathcal{G}_S(T,0) + \mu_o V H^2/2$ is smaller than $G_N(T,H)$. Here $\mu_o V H^2/2$ is the increase in magnetic energy for perfect diamagnetism, $\vec{B} = 0$, inside the sample volume V. This leads to a critical field H_c defined by

$$\mathcal{G}_S(T,0) + \mu_o V H_c^2/2 = \mathcal{G}_N(T,0). \tag{3.3}$$

We assumed that the magnetic energy of the normal state is negligible ($\mathcal{G}(T,H) \approx \mathcal{G}(T,0)$), *i.e.* that its susceptibility is small compared with the perfect diamagnetic response. Above this critical field the sample will be normal. Below it is superconducting. Fig. (3.1) shows some critical curves obtain for elemental superconductors. Since these fields are all less than 150 mT these materials are obviously not used for high field superconducting magnets.

The above discussion works for most of the elemental superconductors, except niobium and vanadium. These last two and most other superconductors do not behave quite as described above. At low field they exhibit a phase of total field expulsion. But after a certain field H_{c1}, called the lower critical field, they allow field to penetrate the sample through a filamentary structure called a vortex. As the field increases, the density of such vortices increases until all the field as penetrated the sample, this happens at H_{c2}, the upper critical field. Beyond H_{c2} the sample is normal again. Between H_{c1} and H_{c2} the sample is said to be in the mixed state or the vortex state. Superconductors displaying this behavior are called type II superconductors while the ones having only the Meissner state and no mixed state are type I superconductors.

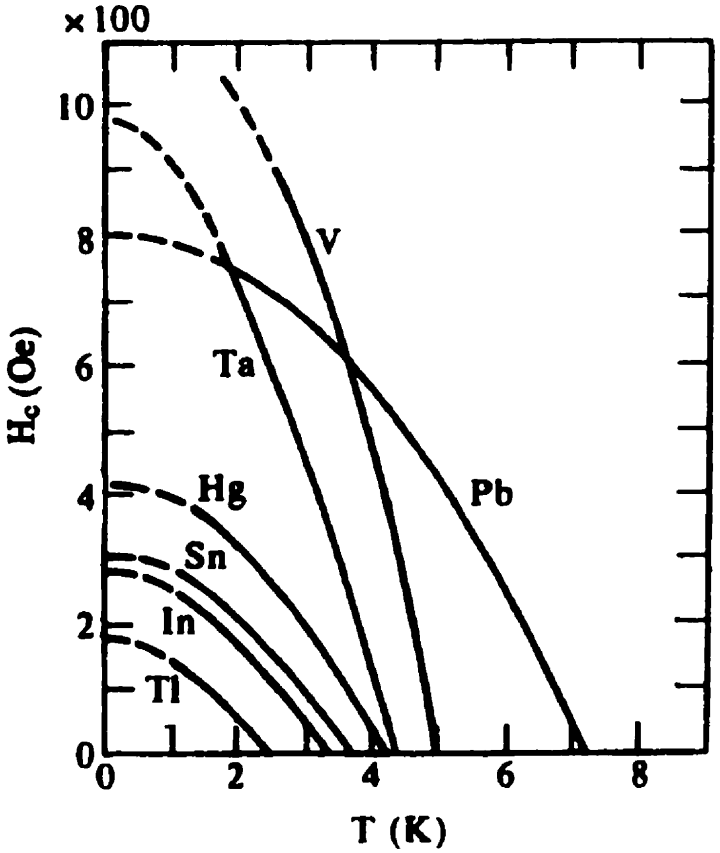

Figure 3.1: Critical field of elemental superconductors as a function of temperature (1000 Oe = 100 mT).

The thermodynamic critical field H_c, described above is now

$$\int_0^{H_{c2}} \mu_o \vec{M} \cdot d\vec{H} = \mathcal{G}_S(T,0) - \mathcal{G}_N(T,0) = -\frac{\mu_o H_c^2}{2} \tag{3.4}$$

for a type II superconductor.

Using the Ginzburg-Landau theory, a precise argument is obtained to distinguish between them. In that theory, the free energy can be written in a dimensionless form. In that form the parameter $\kappa = \lambda/\xi$ plays an important role. When $\kappa < 1/\sqrt{2}$ the material is type I and when $\kappa > 1/\sqrt{2}$ the material is type II. This can be understood as follows. For small κ, the field penetration length is short and the coherence length is long. In the GL theory the coherence length represents the distance over which the order parameter can vary. The order parameter represents the local state of the material. For example if it is close to 1 the volume element is superconducting and if

it is close to 0 the volume element is normal. Hence a long coherence length means the sample supports slowly varying changes from normal to superconducting on the length scale of field variation.

Remember that with respect to the normal state, the energy density of the superconducting state is $U_s^{max} = -\mu_o H_c^2/2$, but that in an applied field $H < H_c$ we must add $U_H^{max} = \mu_o H^2/2$ in the core of the superconductor where $B = 0$. Now imagine the surface of the superconductor where the field decreases rapidly but the sample slowly becomes superconducting, this is the case when $\kappa \ll 1$. In this case U_s and U_H start at 0 but U_s slowly reaches U_s^{max} while U_H rapidly reaches U_H^{max}. This implies that the boundary energy is positive. In the case of large κ, U_H slowly reaches U_H^{max} while U_s rapidly goes to U_s^{max}; this provides a negative energy for the boundary. A negative energy implies that increasing the boundary area can lower the energy of the system. This increase of area can be obtained by having filaments of normal material, through the superconductor, surrounded by this boundary. This is a vortex. Since vortices are quantized there is a minimum energy needed to create a single vortex. This is why the flux does not penetrate before H_{c1}. Of course the GL theory is valid only close to T_c but if κ is large similar results can be obtained over the whole temperature range but with a temperature dependent κ.

Superconductors quantize magnetic flux. This is because the order parameter is complex and must be single valued around a vortex. This implies the quantization of magnetic flux in units of $\phi_o = h/2e = 2.0679 \times 10^{-15}$ Tm^2 (or Weber) where $h = 6.6 \times 10^{-34}$ Js is Planck's constant and $e = 1.6 \times 10^{-19}$ C is the electron charge. The most energetically favorable vortex structure is with a single flux quanta at the core for large κ. Therefore the vortex structure is a tube containing a normal core and a magnetic flux corresponding to ϕ_o.

Above H_{c1} many vortices exist and their interactions tend to organize them in two-dimensional lattices. The most favorable one is triangular but the square lattice is also possible with a little anisotropy of the vortex interaction. Both of these structures have been observed.

A last point about vortices is that they can display hysteretic behavior. The GL description assumed thermodynamic equilibrium. But real materials have defects of all sorts: impurities, lattice defects, etc. All of these can provide a site where the energy to form a normal region (the core) is decreased. Therefore vortices will have a tendency to go there an lower their energy. These defects will act as pinning centers. Once a vortex enters it, it becomes very hard to remove it. This will distort the vortex lattice. Because the vortices must dynamically enter the superconductor from the sample surface they must also exit it that way. A pinned vortex cannot move and therefore the internal field will not be thermodynamically defined. Of course the vortex can get unpinned if it obtains enough energy from thermal fluctuations for example. This is a thermally activated (an exponential law) process and therefore is highly temperature dependent. The activation energy depends on the material and the type of defect. This is important for applications. A moving vortex creates an electrical field and therefore dissipates energy. Therefore in the mixed state without pinning there would not be a perfect conductivity. With pinning, the vortices cannot move and you reobtain perfect conductivity. While type I superconductors have $\mu_o H_c$ of about 100mT, type II superconductors can have $\mu_o H_{c2}$ up to 20 T, or even more.

4

De Haas-van Alphen effect

In this chapter we describe an experiment designed to test the usefulness of the piezoresistive cantilever at low temperatures (< 1K).

The de Haas-van Alphen (dHvA) effect can be used as a sensitive thermometer at low temperature as will be shown below. This allows us to measure the temperature of the sample which rests directly on the cantilever. Because the device is resistive more sensitivity is obtained with more excitation current but this will warm up the device and the sample. So we use the dHvA effect to find out what is the maximum excitation that can be used.

4.1 Theory: de Haas-van Alphen

The de Haas-van Alphen effect is the oscillation of the magnetization of metals as a function of inverse field. The frequency of oscillation is related to the extremum cross sectional area of the Fermi surface (FS). It is therefore a very useful tool in measuring the shape of the FS.

To derive the amplitude of oscillation in the magnetization, or of any other parameter, we calculate the free energy and then take derivatives. We will derive the 2D formula since the systems we have investigated were all two-dimensional.

To obtain the magnetic oscillations in the normal state, we follow Shoenberg [31]. We start by taking into account the quantization of the electron motion due to the magnetic field. This quantization restricts the number of permissible states and is the basic cause of the dHvA oscillations. This can be obtained from the Bohr-Sommerfeld

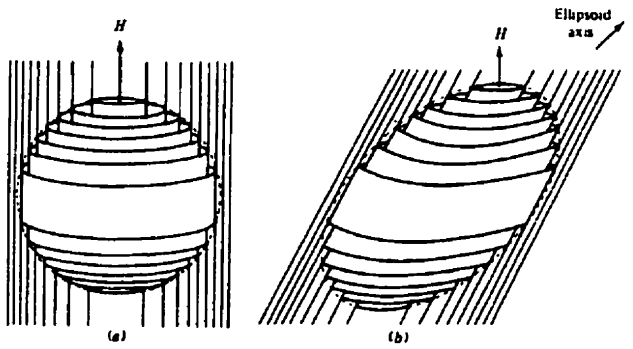

Figure 4.1: Sketches of Landau tubes for *(a)* spherical surfaces of constant energy and for *(b)* ellipsoidal surfaces of constant energy. The Fermi surface is indicated by the broken curve and only parts of the tube inside the FS are occupied at $T = 0$ [31].

quantization rule for periodic motion:

$$\oint \vec{p} \cdot \mathrm{d}\vec{q} = (r + \gamma)2\pi\hbar \tag{4.1}$$

where $\vec{p} = \hbar\vec{k} - e\vec{A}$ for an electron of charge $-e$ ($e = 1.6 \times 10^{-19}$ C) in a magnetic field described by the vector potential $\vec{A}$, and where q is the position of the electron and $\hbar = 1.05 \times 10^{-34}$ Js is Planck's constant. Combining it with the following semi-classical equation:

$$\hbar\dot{\vec{k}} = -e\mu_o(\vec{v} \times \vec{H}) \tag{4.2}$$

where $\vec{v}$ is the electron velocity in a magnetic field $\vec{H}$, we obtain:

$$a(\varepsilon, \kappa) = (r + \gamma)\frac{2\pi\mu_o eH}{\hbar}. \tag{4.3}$$

In eqn. (4.3), a is the area of the orbit in k-space of constant energy ε and with a k component parallel to the field given by κ. This specifies the allowed energy levels (ε_r) in terms of the integer r. These discrete levels are called Landau levels. Fig. (4.1) shows these for a spherical and an elliptical Fermi surface in a magnetic field. Now the constant γ in eqn. (4.3) is unimportant for the oscillations so it is usually given the free electron value of $\frac{1}{2}$.

To obtain oscillations in the magnetization we use the thermodynamic potential defined by:

$$\Omega = \mathcal{G} - N\zeta \tag{4.4}$$

where $\mathcal{G}$ was defined in chapter 2, N is the number of electrons and ζ is the chemical potential. The magnetic moments parallel and perpendicular to the magnetic field are obtained by differentiating the potential:

$$\mathcal{M}_{\parallel} = -\frac{1}{\mu_o}(\partial\Omega/\partial H)_{\zeta}, \tag{4.5}$$

$$\mathcal{M}_{\perp} = -\frac{1}{\mu_o H}(\partial\Omega/\partial\theta)_{\zeta,H}. \tag{4.6}$$

Using Fermi-Dirac statistics we express the free energy in terms of the allowed energy levels:

$$\Omega = -k_B T \sum \ln\left(1 + \mathrm{e}^{(\zeta-\epsilon)/k_B T}\right) = -k_B T \int_{\infty}^{\infty} \mathrm{d}\kappa \left(\frac{\mu_o e H V}{2\pi^2\hbar}\right) \sum_r \ln\left(1 + \mathrm{e}^{(\zeta-\epsilon_r)/k_B T}\right) \tag{4.7}$$

where $k_B = 1.38 \times 10^{-23}$ J/K is Boltzmann's constant. In the transformation from summation to integration, the degeneracy of the levels is needed. At $H = 0$, remembering that there are 2 spins per k-state, the density of k-states is $V/4\pi^3$ where V is the real space volume. So defining $\Delta a \equiv a(\varepsilon_{r+1}, \kappa) - a(\varepsilon_r, \kappa) = 2\pi\mu_o eH/\hbar$ from eqn. (4.3) we obtain that the degeneracy(D) of states for a particular r between κ and $\kappa + \mathrm{d}\kappa$ is

$$D = \Delta a\, \mathrm{d}\kappa V/4\pi^3 = \mu_o e H V \mathrm{d}\kappa/2\pi^2\hbar \tag{4.8}$$

After some manipulations at $T = 0$ and keeping only the oscillating term, which we denote by $\tilde{\Omega}$:

$$\tilde{\Omega} = \frac{\mu_o e \omega_c H V}{4\pi^2} \int \mathrm{d}\kappa \sum_{p=1}^{\infty} \frac{1}{\pi^2 p^2} \cos\left\{2\pi p \left(\frac{\mathcal{A}(\kappa)\hbar}{2\pi\mu_o eH} - \frac{1}{2}\right)\right\} \tag{4.9}$$

where p labels the harmonic, $\omega_c = \mu_o eH/m = 0.176\mu_o H/m$ is the cyclotron frequency (the number gives ω_c in THz=10^{12}Hz and assumes $\mu_o H$ is given in Tesla and m is given in units of $m_e = 9.1 \times 10^{-31}$ kg), $m = \hbar^2(\partial a/\partial\varepsilon)_{\kappa}/2\pi$ is the effective mass and $\mathcal{A}$ is the Fermi surface area. When differentiating the free energy to get the magnetization a saw-tooth waveform is obtained. This can be explained by the change in last occupied Landau level. As the magnetic field is increased, the Landau level moves toward the Fermi energy, this makes the magnetization increase. Once the level crosses the Fermi

energy it becomes unoccupied, since we are at $T = 0$, which gives a sudden change in magnetization.

In a two dimensional system $\mathcal{A}$ is independent of κ. So if the integral is done over one unit cell of height d hence κ varies from 0 to $2\pi/d$, and that we take the derivative to obtain the magnetization only on the rapidly changing part of the free energy, the cosine, because that gives the most important contribution we obtain the oscillating magnetic moment $\tilde{\mathcal{M}}_{\|}$

$$\tilde{\mathcal{M}}_{\|} = -\frac{V}{\mu_o d}\frac{eF\omega_c}{\pi^2 H}\sum_{p=1}^{\infty}\frac{1}{p}\sin\left\{2\pi p\left(\frac{F}{\mu_o H}-\frac{1}{2}\right)\right\}. \tag{4.10}$$

Where $F = (\hbar/2\pi e)\mathcal{A}$ is the dHvA frequency. If we write F in kT and $\mathcal{A}$ in Å^{-2} then $F = 10.5\mathcal{A}$. Also if we assume a circular orbit then the fermi velocity v_F is given by

$$v_F = \frac{\hbar k_F}{m} = \frac{\hbar}{m}\sqrt{\frac{\mathcal{A}}{\pi}} = \frac{1}{m}\sqrt{2e\hbar F} = 2.02\times 10^5\frac{\sqrt{F}}{m} \tag{4.11}$$

where at the end we express F in kT, m in units of m_e and obtain v_F in m/s. Finally if we still assume a circular orbit we have that the radius of the orbit in real space, r_o, is

$$r_o = \frac{v_F}{\omega_c} = \frac{1}{\mu_o H}\sqrt{\frac{2\hbar F}{e}} = 1.15\frac{\sqrt{F}}{\mu_o H} \tag{4.12}$$

where again F is in kT, $\mu_o H$ is in Tesla and r_o is in μm.

In a 2D system the angular dependence of the frequency and of the effective mass are the same and are derived from geometrical considerations. This gives

$$F(\theta) = \frac{F(0)}{\cos(\theta)}, \tag{4.13}$$

$$m(\theta) = \frac{m(0)}{\cos(\theta)} \tag{4.14}$$

where θ is the angle the field makes away from the vector normal to the plane. Also d is angle dependent and is given by $\frac{2\pi}{d(\theta)} = \frac{2\pi\cos(\theta)}{d(0)}$.

Using this we can find the perpendicular magnetization and the torque signal. Again we take the derivative only on the rapidly varying part of the free energy and we obtain:

$$\tilde{\mathcal{M}}_{\perp} = \frac{-1}{F}\frac{dF}{d\theta}\tilde{\mathcal{M}}_{\|} \tag{4.15}$$

$$\tilde{\tau} = \mu_o H \tilde{\mathcal{M}}_\perp = -\mu_o H \frac{1}{F}\frac{dF}{d\theta}\tilde{\mathcal{M}}_\parallel \tag{4.16}$$

which are general results valid also in 3D. In 2D $\frac{1}{F}\frac{dF}{d\theta} = \tan(\theta)$ so $\tilde{\mathcal{M}}_\perp = \tilde{\mathcal{M}}_\parallel \tan(\theta)$ and $\tilde{\tau} = \mu_o H \mathcal{M}_\parallel \tan(\theta)$.

In 3 dimensions, the κ dependence of $\mathcal{A}$ in eqn. (4.9) makes the integration mix many different frequencies. This smearing is smallest for extrema of the cross-section so the integration will pick out these extrema because they will contribute the most and we obtain

$$\tilde{\mathcal{M}}_\parallel = -\left(\frac{e}{\hbar}\right)^{3/2} \frac{FV\hbar\omega_c}{(2\pi^5\mu_o H A'')^{1/2}} \sum_{p=1}^{\infty} \frac{1}{p^{3/2}} \sin\left[2\pi p\left(\frac{F}{\mu_o H} - \frac{1}{2}\right) \pm \frac{\pi}{4}\right] \tag{4.17}$$

where $F = (\hbar/2\pi e)A$ is the dHvA frequency and A is an orbit extremum. The $\pm$ sign depends on whether the extremum is a maximum(-) or a minimum(+) and A'' is $|\partial^2\mathcal{A}/\partial\kappa^2|_{\kappa=0}$. For a spherical Fermi surface $A'' = 2\pi$.

Finally we must include the effects of finite temperature, impurity scattering etc. This can be done in a similar way as for the 3D integration. This is because all these effects can be seen as replacing a well defined F with a certain distribution. The temperature affects the Fermi function by removing the sharp cutoff in occupation of Landau tubes at the Fermi energy. The impurity scattering which gives a finite lifetime for the quasiparticles, will give a Lorentzian distribution to F. Even the effect of having spin up and spin down electrons which have a different energy in the magnetic field can be included by saying there are two very close F, one for each spin. So all these effects are seen to affect the phase of the signal with a certain probability distribution. Fourier analyzing these distributions we obtain R_T, the temperature reduction factor, R_D the Dingle factor due to impurity scattering and R_s the spin factor:

$$R_T = \frac{2\pi^2 p k_B T/\hbar\omega_c}{\sinh(2\pi^2 p k_B T/\hbar\omega_c),} \tag{4.18}$$

$$R_D = \exp(-\pi p/\omega_c\tau_o) = \exp(-2\pi^2 p k_B T_D/\hbar\omega_c) = \exp(-\pi p r_o/l_o) \tag{4.19}$$

and

$$R_s = \cos\left(p\frac{\pi}{2}g\frac{m}{m_e}\right) \tag{4.20}$$

where T_D is the Dingle temperature, τ_o is the scattering rate, l_o is the scattering length and g is the spin-splitting factor (for free electrons $g = 2.0023$). For large temperatures, R_T can be expressed as an exponential and this similarity to R_D is the reason why the scattering is often given as a temperature (T_D). If we express $\mu_o H$ in Tesla, m in m_e and T in Kelvin we obtain that

$$R_T = \frac{14.69pmT/\mu_o H}{\sinh(14.69pmT/\mu_o H)} \tag{4.21}$$

and

$$R_D = \exp(-14.69pmT/\mu_o H). \tag{4.22}$$

Also we have that the scattering rate ($\Gamma = \tau_o^{-1}$), is related to T_D by $\Gamma = 2\pi k_B T_D/\hbar = 0.823T_D$ where Γ is in THz. We should note that at very low temperature, we should be in the impurity scattering limit where it is the scattering length (l_o) which is constant. It is related to T_D by $l_o = v_F\tau_o = 0.245\sqrt{F}/mT_D$ where we give l_o in μm using F in kT, T_D in K and m in m_e.

In a similar way, other cause of phase smearing, such as field inhomogeneity, can be calculated [31].

Putting everything together we obtain the LK formula for the magnetic moment of a 2D system to be:

$$\tilde{\mathcal{M}} = -\frac{V}{\mu_o d}\frac{eF\omega_c}{\pi^2 H}\sum_{p=1}^{\infty}\frac{R_T R_D R_s}{p}\sin\left\{2\pi p\left(\frac{F}{\mu_o H}-\frac{1}{2}\right)\right\}. \tag{4.23}$$

If more than one frequency is present, they all obey the LK formula separately and the measured oscillation is the sum of those contributions.

Before ending this section, we mention that in the superconducting state, oscillations can still be measured. For example in 2H-$NbSe_2$, oscillations have been observed down to $0.3H_{c2}$ [32, 33]. Upon entering the mixed the Dingle temperature increases. In some materials it increases very quickly which makes observation at a small fraction of H_{c2} impossible but in some others the additional scattering is small. This additional scattering is present because of the superconducting state. The vortices provide a certain field inhomogeneity and the coupling between electrons between

different Landau levels produces a phase smearing effect. A few theories have been put forward [34, 35, 36] to explain this but there is still no definite explanation.

4.2 Experimental technique

The amplitude of the de Haas-van Alphen oscillations decreases rapidly has the magnetic field is decreased or the temperature is increased. The sample we have studied required temperatures below 1K and fields above 5T to make the observation of the dHvA effect possible. Therefore the experiments were carried out in a dilution refrigerator equipped with a superconducting magnet. Good references for low temperature techniques are [37, 38, 39, 40].

4.2.1 Dilution refrigerator

The dilution fridge we used is an Oxford Kelvinox 300 dilution refrigerator (see fig. (4.2)). It is equipped with a 15 T superconducting magnet with a compensated region centered on the bottom plate of the mixing chamber. In the compensated region the field stays below 5 mT. Therefore we can place there our principal thermometer, a germanium sensor from Lakeshore. This GR-200A-30 is calibrated between 50 mK and 5 K. Without the compensated region this sensor would be affected by the field and the temperature would not be known, at least from that sensor.

The dilution refrigerator cools by taking advantage of the properties of a mixture of ^{3}He and ^{4}He [20, 39]. When the mixture is cooled below 0.87 K a phase separation occurs. An almost pure liquid ^{3}He phase floats on top of a phase with approximately 6% of ^{3}He in superfluid ^{4}He. The top layer is called the concentrated phase and the bottom the dilute phase. The reason for the mixed phase is due to quantum statistics. The ^{4}He is a boson. At 4.2 K it becomes a liquid under atmospheric pressure. Under lower pressure the boiling point is lower. This enables cooling of the liquid by pumping on it. This method can reach about 1 K before the pressure is too small to be lowered further. At 2.2 K, for pressures of 1 bar and less, a Bose condensation occurs and it becomes superfluid. This state has a non-zero fraction of

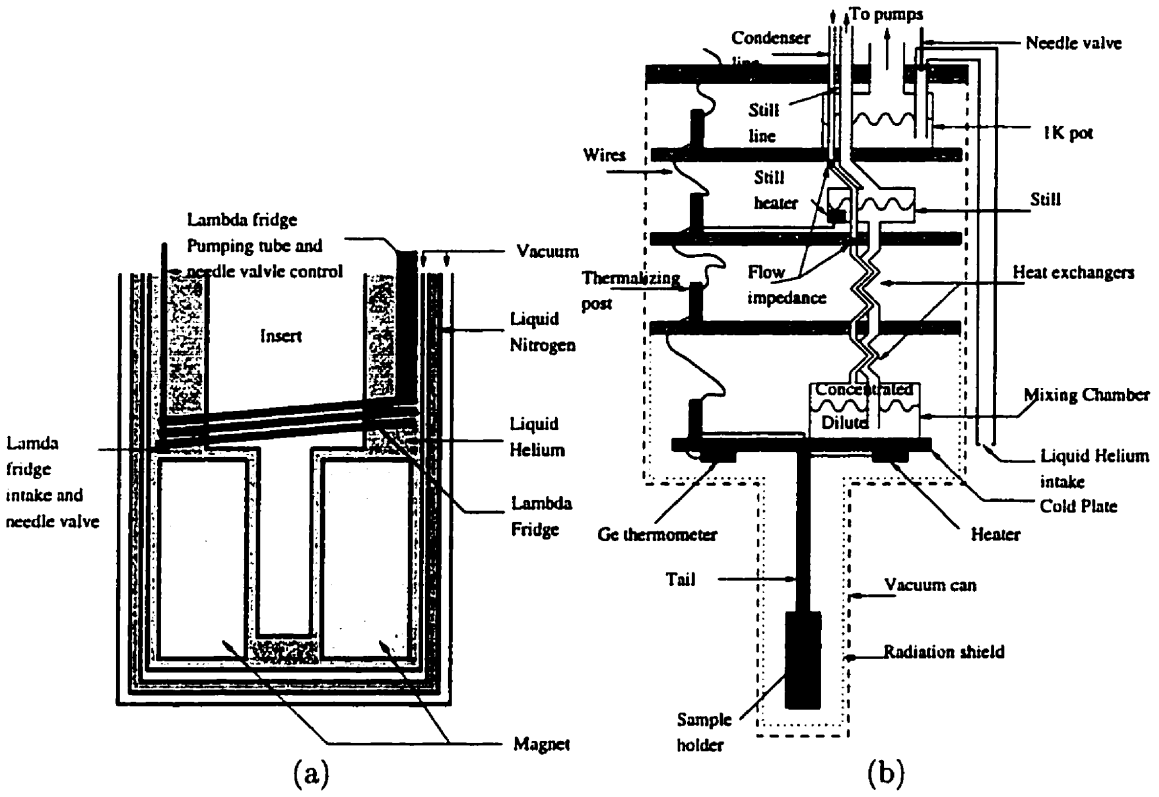

Figure 4.2: (a) shows the position of the magnet and of the lambda fridge. (b) shows the insert and the dilution unit. Note that the diagrams are not to scale.

the atoms in the ground state. It also has strange behaviors. Below 0.5 K most of the atoms are in the ground state and it is therefore thermodynamically inert.

The ^{3}He is a fermion. It is a gas under normal pressure until 3.2 K when it becomes liquid. Like for ^{4}He at lower pressure it has a lower boiling point. By pumping on it, a temperature of about 0.3 K can be reached. But it does not Bose-condense into a superfluid since it is a fermion.[1]

By placing ^{3}He atoms into liquid ^{4}He their energy is lowered. Thats why even at 0K they still mix. Also the liquid ^{4}He is like vacuum for the ^{3}He since it is inert.

The cooling is obtained by removing ^{3}He from the dilute phase. Then some ^{3}He from the concentrated phase will go into the dilute phase. This cools the mixture in the same way pumping the vapor of liquid Helium cools the liquid. The actual procedure is to precool the mixture by putting it into contact with a 1K pot, a pot

[1]It does have a transition to a superfluid phase. Like in superconductors the fermions form pairs and it is these pairs which condense. This occurs below 3 mK and is irrelevant in the dilution fridge.

filled with He on which we pump attaining about 1K. Then the mixture goes into the mixing chamber were the phase boundary occurs. There a tube takes the dilute phase into the still. The still is heated to evaporate the ^{3}He, which is then pumped in a close system and reinserted to the concentrated phase in the mixing chamber. This is a closed circuit. Two more details: in the condenser line, where the liquid goes back into the mixing chamber, there are flow impedances to increase the pressure in the pot and the still to help the cooling. Also heat exchangers between the mixing chamber and the still are essential to attain low temperatures.

The base temperature of the fridge is 10 mK. All the wiring is thermally anchored at all of the cold stages. Temperature control is done by measuring the resistance with a LR-700 resistance Bridge from Linear Research. This signal is used to control the power to a heater using the TS-530 temperature controller from RV-electronikka. The heater is also in the compensation zone but is far away from the Germanium thermometer.

The magnetic field is produced by the superconducting magnet. It can provide vertical fields up to 13 T at 4.2 K. When the liquid helium around the magnet is cooled further down to 2.2 K it then can go up to 15 T. To attain this a lambda fridge is used. This is a tube in the form of a coil which is placed just above the magnet. One end of it has a hole with a needle valve. The other side goes to an external pump. With the valve open, liquid helium enters the tube, and pumping on it cools it down to 2.2 K. This eventually cools all the liquid below; above the coil the liquid stays around 4 K. This is more economical than pumping on the whole bath, where all the liquid gets cooled down. Even this way a good fraction of liquid helium gets lost. In our experiments so far we have not used the magnet with the lambda fridge, so the highest field we have used is 13 T.

High fields were obtain using the PS-120 power supply from Oxford which can deliver 120 A and is limited to 10 V.

4.2.2 *Electronics*

The measurement of the signal is quite simple. All that is needed is to measure the resistance of the piezoresistive cantilever. This could be done with a resistance bridge like the LR-700. But such a device has a fixed operating frequency and its discretization limits us. Therefore we used a digital lock-in amplifier, the SR-850 from Standford Research. These supply a reference voltage between 0.004 V_{RMS} and $5V_{RMS}$ at a frequency ranging from 5 mHz to 100 kHz. We have used frequencies from about 10 Hz to 4 kHz. This reference signal goes through a large resistor followed by the piezoresistance to ground. The large resistance is a current limiting resistance. It is chosen to be large (100 kΩ or 1 MΩ) compared to the piezoresistance (about 2.5 kΩ). Under these conditions the current stays constant to first order under small changes in the piezoresistance.

The resistance is measured by taking the voltage difference across the piezoresistance (fig. (4.3)). This is then detected in the lock-in. This device extracts the in phase and out of phase components of the measured signal in a small bandwidth at the reference frequency. This is done by multiplying the measured signal by the reference and a 90° phase shifted reference and filtering the output. With a signal $V\sin(\omega t+\phi)$ and a reference $\sin(\omega_o t)$ we obtain

$$V\sin(\omega t+\phi)\sin(\omega_o t)=\frac{V}{2}\left[\cos(\omega t+\phi-\omega_o t)-\cos(\omega t+\phi+\omega_o t)\right] \tag{4.24}$$

and

$$V\sin(\omega t+\phi)\cos(\omega_o t)=\frac{V}{2}\left[\sin(\omega t+\phi+\omega_o t)-\sin(\omega t+\phi-\omega_o t)\right]. \tag{4.25}$$

Hence if the signal is at the same frequency as the reference ($\omega=\omega_o$) then we obtain a DC signal and a signal at $2\omega_o$. These signals then go through low pass filters. The filtering removes the $2\omega_o$ signal. The filtering is important also to lower the noise, since it selects the bandwidth. The smaller the bandwidth the smaller the noise. Therefore we used a bandwidth of 1 Hz or less.

The above technique works but it has a limited sensitivity. The lock-in digitizes the signal and you can only measure to 1 part per 5×10^4. Anything smaller will

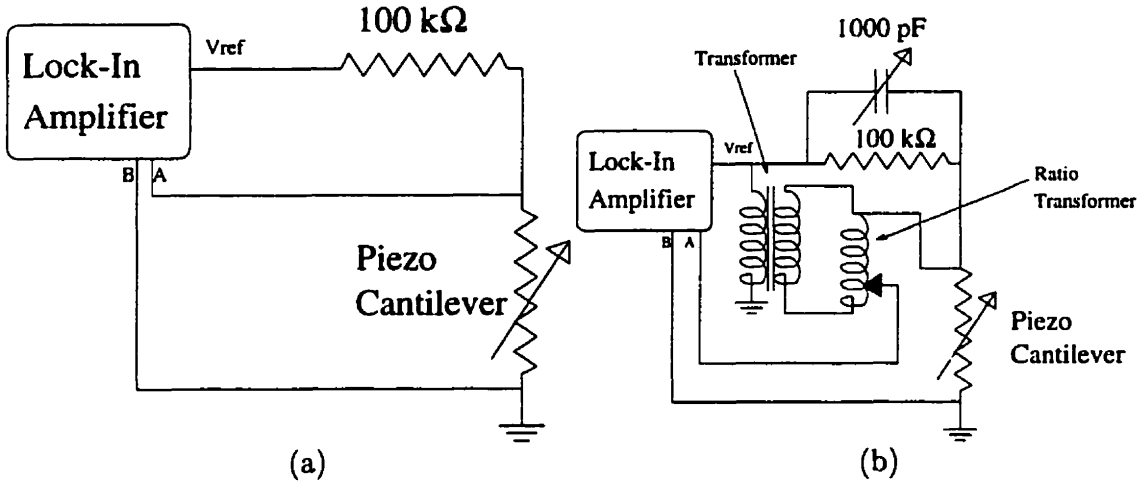

Figure 4.3: (a) Simplest circuit used. (b) Improved circuit using a ratio transformer.

be lost in the last bit. The solution to this problem is to make the full scale signal smaller. This can be done by subtracting a fraction of the input signal to one of the inputs. We did this using only passive elements (fig. (4.3)). A transformer is used to isolate a ratio transformer. The tap of the ratio transformer allows us to select a fraction of the reference voltage with an accuracy of 0.1 ppm. The floating ratio transformer is referenced to the high voltage side of the piezoresistance. The tap is then at $V_{\text{top piezo}} - xV_{\text{ref}}$, where x is the fraction. Of course the bottom voltage could also be raised close to the top one but it is better to lower the top one. This lowers the common mode signal to the differential amplifier on the input of the lock-in. These differentials amplifiers have a large but finite common mode rejection ratio of 100 dB at 1 kHz. Therefore if the common signal is too large, it will affect the differential signal.

The insulating transformer and the ratio transformer both require medium frequency to operate (100 Hz to 15 kHz). Therefore when these are used no low frequency measurement can be taken. This frequency causes the parasitic capacitances to start becoming a problem. The wires consist of closely wound twisted pairs of copper, superconducting and or manganin wires in the fridge and of coaxial cables

outside. All these have capacitances. These make the signal have a large phase shift as the frequency is increased. The ratio transformer technique above only removes an in phase component therefore if the phase shift reaches 45°, removing the in phase will not help. The out of phase signal must therefore be controlled and that is the purpose of the adjustable capacitor placed in parallel to the limiting resistor.

It should be noted that the current can be measured. A small resistance (1 kΩ) is placed between the piezoresistance and ground. Then the voltage across it is measured using a second lock-in which uses the reference signal of the first lock-in. It is necessary to use this technique if the limiting resistor is cooled, *i.e.* is in the fridge. This was done in some cases, but as the temperature changes, the value of the limiting resistance changes, so it is absolutely necessary to measure the current in this case.

We should note that below 1 K we achieved a sensitivity of 10 mΩ, which is equivalent to 10 Å or 4 ppm or 10^{-12} Nm. This is equivalent to a magnetic moment of 10^{-13} Am^2 at 10 T. We have to compare this to the standard method to measure the dHvA effect: the modulation technique. This is an inductive method where a steady high magnetic field and a small AC field are applied to the sample. This makes the magnetization vary in time and the induced e.m.f. in a balanced pair of pick-up coils is measured. By selecting a large amplitude of modulation this technique measures directly the oscillating magnetization ($\tilde{\mathcal{M}}_{\parallel}$). At lower amplitudes it measures derivatives ($d^n\tilde{\mathcal{M}}_{\parallel}/dH^n$). For the most favorable coil geometry, field modulation amplitude and frequency, that technique could theoretically achieve a sensitivity of 10^{-15} Am^2 [31]. Of course in practice it is difficult to achieve such a sensitivity because of the vibrations produced by the field modulation and because inductive noise is picked up. A final point about the comparison, since the torque measures $H\tilde{\mathcal{M}}_{\parallel}\frac{1}{F}\frac{dF}{d\theta}$ as the field is increased or for large anisotropy the sensitivity is increased. This is not the case for the modulation technique.

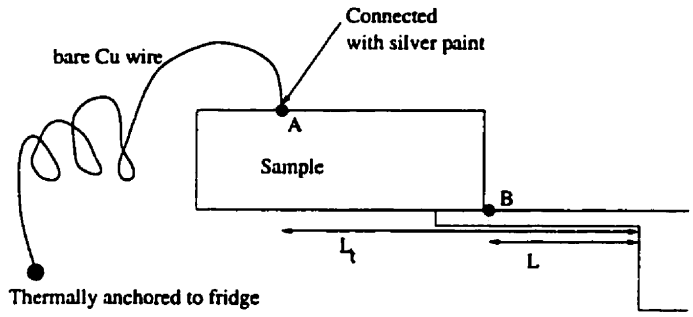

Figure 4.4: Diagram showing mounted sample with thermalizing wire.

4.2.3 *Sample mounting*

Before ending this section we must look at the mounting of the crystals. The crystals are attached to the piezo using vacuum grease (Dow Corning High vacuum grease). But since we want to use a large excitation current in the piezo and possibly warm it up, we would like to keep the sample cold. We achieve this by attaching a thermalizing wire to the sample as is shown in fig. (4.4). This thermalizing wire needs to conduct heat well but be very flexible so that it does not affect the spring of the cantilever. This is obtained by using a 50 μm diameter, or smaller, copper wire of about 2 cm, coiled. It is stripped from any insulation to make it more flexible without affecting the thermal conduction. It is attached to the sample using silver paint, and soldered to the sample mount on the other side.

The thermalizing wire modifies the spring constant. The change is given by

$$K_{eff} = K + \left(\frac{L_t}{L}\right)^2 K_t \tag{4.26}$$

where K is the spring constant of the cantilever at point B and K_t is the spring constant of the thermalizing wire at point A. L and L_t are defined in fig. (4.4). Therefore to limit the effect of the thermalizing wire on the spring constant it should have $K_t \ll K(L/L_t)^2$. Now if we use $K = 20$ N/m, $L = 150$ μm and $L_t = 600$ μm we obtain the restriction that $K_t \ll 1.2$ N/m.

We can estimate K_t using eqn. (2.10) ($K = 3EI/L^3$) of chapter 2 and using $I = \pi r^4/4$. Here $E = 1.0 \times 10^{11}$ N/m [41], $r = 25$ μm and $L = 2$ cm. This gives $K_t = 1.1 \times 10^{-2}$ N/m which is smaller than the restriction derived above. Of course

this calculation assumed that the wire is straight. This is not the case here, the wire is bent in a few loops, but the order of magnitude won't change.

The sample holder is then placed close to the middle of the field region. Since the torque measurements need to be at an angle, the sample holder is placed at an angle of about 25 to 30° which should provide optimum dHvA signals for the samples we measured.

4.3 Samples

The main criteria for their selection was that they should be anisotropic. Anisotropy is needed to do a torque measurement. For the de Haas-van Alphen experiment this requires that the Fermi surface should be anisotropic. Two dimensional systems have a large FS anisotropy and their dHvA signal is enhanced compared to 3 dimensional system. Therefore we choose 2D systems. It also turns out that both samples we measured were superconductors. This was not a prerequisite but we are a superconductivity group after all and the dHvA effect in the mixed state of superconductors is interesting in its own respect.

4.3.1 Organic superconductor

The first sample we measured was an organic superconductor. This is one of the three classes of unconventional superconductors. The other two are the heavy fermions, like UPt_3, which were discovered in the late 1970's, and the high-T_cs, like $YBa_2Cu_3O_{7-\delta}$ and $La_{2-x}Sr_xCuO_4$ which were discovered in 1986. The organic superconductors were discovered in 1980. They all have a very rich phase diagram (see [42, 43]). There exist two main groups. The first group is the quasi one-dimensional systems. Most of these are $(TMTSF)_2$-X, the X represents an anions which through charge transfer with the TMTSF molecule provides free carriers which render the system conducting. By applying pressure, or choosing different anions, the materials can be changed from an antiferromagnetic state to a superconducting state to a spin density wave (SDW) state. The maximum T_c is about 1 K. The only compound which is superconducting

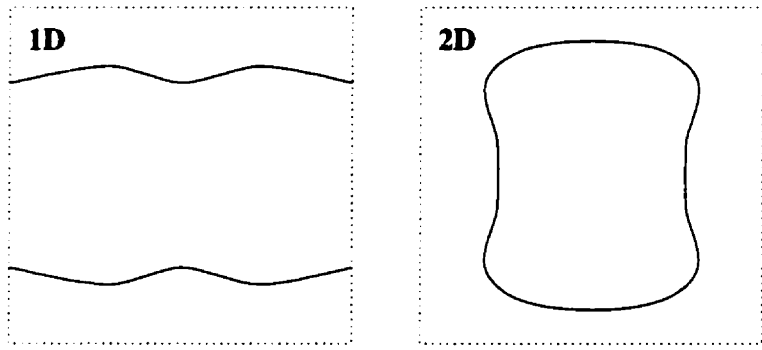

Figure 4.5: Fermi surface example of 1D and 2D systems.

under atmospheric pressure is $(TMTSF)_2ClO_4$. The others need some pressure to become superconducting.

Since these are one-dimensional their Fermi surfaces are open (fig. (4.5)). They are two undulating sheets. Therefore they cannot be observed by the dHvA effect since it needs closed orbits.

The other group is the 2 dimensional one. They are based on the bis(ethylene-dithiolo)tetrathiafulvalene (BEDT-TTF) molecules or ET for short. Again, combining them with anions, a charge transfer occurs and leaves free electrons. These are also sensitive to pressure. The highest ambient pressure T_c is 11.6 K for κ-$(ET)_2Cu[N(CN)_2]Br$ [44, 45]. The second highest is 10.4 K for κ-$(BEDT\text{-}TTF)_2Cu(NCS)_2$ [5]. These systems, being two dimensional tend to have closed Fermi surfaces which are cylindrical. κ stands for the phase of the material. The ET molecules can stack in different orders and these are represented by Greek letters. For example $(ET)_2I_3$ as been studied in the α, β, γ, θ and κ phases (see references in [5]). An example of the high sensitivity to pressure of these compounds is that $dT_c/dP \approx 3 - 36$ K/kbar which is higher than any other system including the high-T_c's [46]. The highest T_cs have been observed in the κ phase.

Many observations of the Fermi surface have been done on these materials. Several techniques have been used: modulation technique, capacitive torque, Shubnikov-de Haas (observations of oscillations in the resistance), etc. Of the κ phase, $(ET)_2I_3$ [47], $(ET)_2Ag(CN)_2H_2O$ [48] and $(ET)_2Cu(NCS)_2$ [49, 50, 51, 52, 53] have been mea-

sured. The surface of $(ET)_2Cu[N(CN)_2]Br$ as been observed with the Shubnikov-de Haas effect but only under pressures above 9 kbar [54]. This pressure removes the superconductivity. The experiment obtained a frequency 4 times smaller than band calculations and a very small amplitude. No ambient pressure measurement of the FS have been reported. This can be due to the high upper critical of about 15 T (obtained by a capacitive torque method [55]) which makes a dHvA experiment impractical. Ching *et al.*, along with a band structure calculation explained the difficulty of measurement using magnetic oscillations by the fact that multiple sheets of the FS are very close together and have a small effective mass [56].

We have measured κ-$(BEDT\text{-}TTF)_2Cu(NCS)_2$. The ET molecules are stacked in the *b*-*c* plane of the crystal. In the *a* direction of the crystal the ET planes are separated by a $Cu(NCS)_2^-$ anions layer. The *b*-*c* plane is where metallic and superconducting behavior occur. The crystal structure is monoclinic with $a = 16.25$ Å, $b = 8.44$ Å and $c = 13.12$ Å at room temperature [57]. Fig. (4.6) shows the crystal structure and fig. (4.7) shows its Fermi surface. In [58] it is obtained by a self-consistent orthogonalized linear combination of atomic orbitals (OLCAO) method based on the local approximation of the density functional theory. It consists of 3 surfaces: two undulating sheets and a small ellipse. Under high enough field (above 14 T) magnetic breakdown occurs. In that case electrons can jump from the sheets to the small ellipsoid and therefore a large orbit appears [49, 52]. Since we did not go to those fields we should observe only the small orbit. Table (4.1) shows the parameters for this small orbit.

The many different dHvA measurements have focussed on different aspects. Swanson *et al.* observed flux jumps in the mixed state and also observed an estimated the anisotropy of the material by finding the amount of warping on the side of the cylindrical FS [50]. Meyer *et al.* have looked at the high field magnetic breakdown and also at the angular dependence of the amplitude. From this they extract $g = 1.6$ as the parameter in the spin reduction factor of the LK formula [49]. Also P.J. van der Wel *et al.* looked at it close to H_{c2} and observed a few oscillations in the mixed state

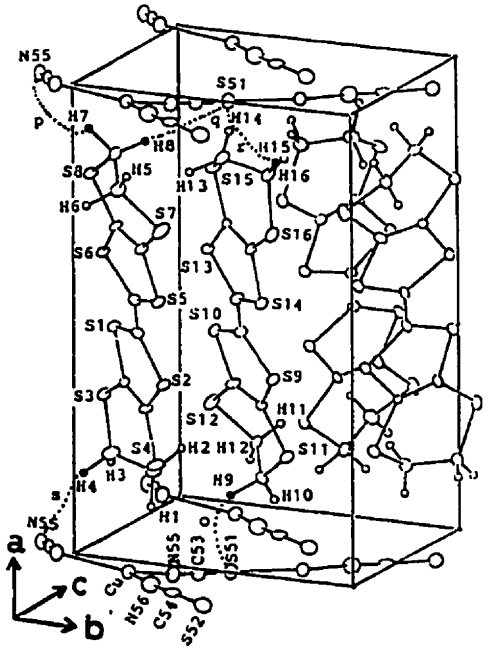

Figure 4.6: Crystal structure of κ-(BEDT-TTF)$_2$Cu(NCS)$_2$ [5].

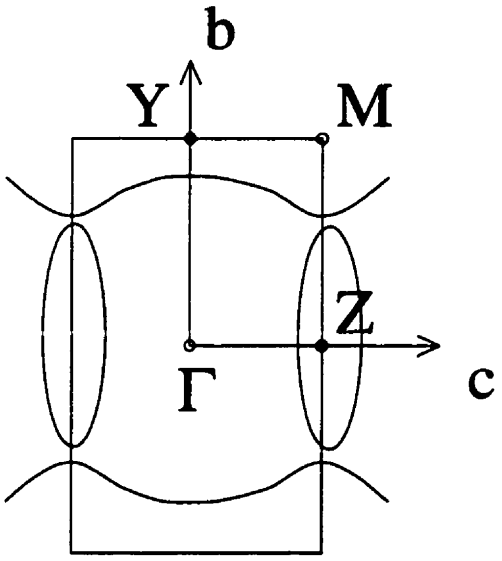

Figure 4.7: Fermi surface of κ-(BEDT-TTF)$_2$Cu(NCS)$_2$.

[51].

This material is ideal for the purpose of testing the piezo. It's signal should be big enough to see and its effective mass should make it a good thermometer in the 100 mK to 1 K range. It's upper critical field is about 5 T [50] which is low enough

Frequency F (kT)	0.601
Cyclotron mass (m_e)	3.2
Band calc. F (kT)	0.45
Band mass (m_e)	1.7

Table 4.1: Measured ([49]) and calculated ([58]) Fermi surface parameters for κ-(BEDT-TTF)$_2$Cu(NCS)$_2$.

to permit the experiment but large enough that we can hope to see some oscillations in the superconducting state. The crystals are of high quality, *i.e.* their impurity scattering rate is small (they have a mean free path of about 0.2 μm). One caution is that the samples are very fragile so they must be mounted with care.

The sample we used was supplied by Dr. K. Behnia of the CNRS at Orsay, France. It was grown by a standard electrochemical technique [5]. It was a platelet of regular thickness but irregular shape. It had dimensions of roughly $750 \times 450 \times 40$ μm. These dimensions were estimated using a caliper and by comparison with small wires of known diameter.

4.3.2 Sr_2RuO_4

The other material we investigated is Sr_2RuO_4. This material has been around at least since 1959 [59]. But since the recent discovery that it is a superconductor below 1 K by Y. Maeno *et al.* [6] it has attracted a lot of attention. This discovery was possible because of the availability of very high quality crystals. This is important since the superconductivity in this material disappears quickly with just a few parts per million (ppm) of impurity.

The interest in this material is that its crystal structure [6, 59, 60] is the same as that of $La_{2-x}Sr_xCuO_4$ which is one of the high-T_c compounds (see fig. (4.8)). In these high-T_c materials the superconductivity is believed to occur in the CuO_2 planes. Since Sr_2RuO_4 does not contain copper it can give some insight on the role of Cu

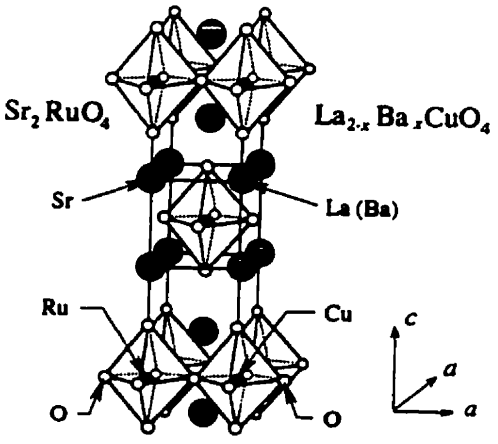

Figure 4.8: Crystal structure of Sr_2RuO_4. The lattice parameters are $a = b = 3.87$ Å and $c = 12.74$ Å [6].

in the high-T_c. In $La_{2-x}Sr_xCuO_4$ superconductivity occurs only with some doping (x=0.06–0.25) while with x=0 it is an antiferromagnetic insulator. This is in contrast to Sr_2RuO_4 which is a superconductor without any doping. In fact upon doping with iridium, $Sr_2Ru_{1-x}Ir_xO_4$ stops being a metal above x=0.1 and becomes an insulator above x=0.6; Sr_2IrO_4 shows a weak ferromagnetism [61]. Also it does not have structural transitions below room temperature unlike $La_{2-x}Sr_xCuO_4$ (see [60] and references therein).

The low temperature specific heat, AC susceptibility, resistivity [6, 62, 63] and a few other experiments like dHvA (to be described later) seem in accordance to Fermi liquid theory. If this is the case, it tests the limits of applicability of the theory because it is a highly two dimensional system. For example the ratio of the resistivity perpendicular and parallel to the plane exceeds 500.

Experiments on the specific heat in the superconducting state, the mass enhancement obtained from dHvA and a few other experiments seem to indicate an unconventional superconducting paring state. Some theorists propose that the superconductivity in this material might be similar to the superfluidity of ^{3}He, which is p-type. Other explanations have also been proposed (see [64] and references therein).

Fig. (4.9) shows the Fermi surface based on the local-density approximation (LDA)

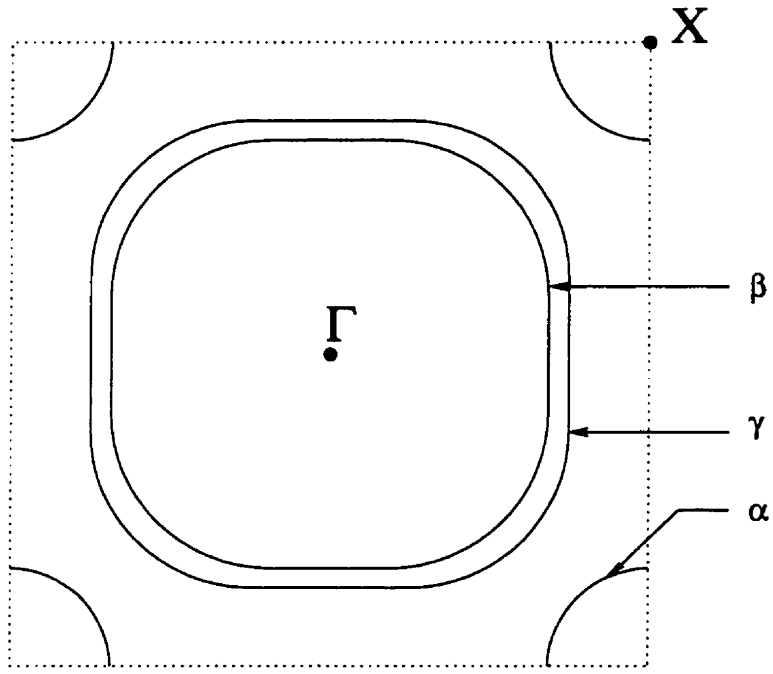

Figure 4.9: Fermi surface of Sr_2RuO_4.

to density-functional theory using a self-consistent linear-augmented-plane-wave (LAPW) method [65, 66, 67, 68]. It shows three sheets. The α sheet is a hole-pocket while the other two, β and γ, are electron-pockets. Two type of experiments where performed on this to measure the Fermi surface. A standard dHvA experiment was performed by Mackenzie *et al.* and they observed a Fermi surface which is consistent with the theoretical prediction [69]. Table (4.2) shows the theoretical and experimental values obtained. The difference between the theoretical and experimental effective mass implies strong electron correlations. The assignment of hole or electron to the pockets is done using a measurement of the Hall effect [70]. The same group also used the measured Fermi surface to predict the electronic specific heat, the resistivity and the upper critical field [71]. These predictions agree well with experiments.

The other type of experiment used to measure the Fermi surface is angle-resolved photoemission spectroscopy(ARPES). This is a surface probe. It measures only in the top few nanometers of material while the dHvA effect is a bulk measurement. ARPES was done on Sr_2RuO_4 by two groups at temperatures above 20K [72, 73].

	α	β	γ
Frequency F (kT)	3.05	12.7	18.5
Average k_F (Å^{-1})	0.302	0.621	0.750
$\Delta k_F/k_F$ (%)	0.21	1.3	<0.9
Cyclotron mass (m_e)	3.4	6.6	12.0
Band calc. F (kT)	3.4	13.4	17.6
Band calc. $\Delta k_F/k_F$ (%)	1.3	1.1	0.34
Band mass (m_e)	1.1	2.0	2.9

Table 4.2: Measured and calculated Fermi surface parameters for Sr_2RuO_4 [69].

They both obtained a Fermi surface which is different then the theoretical one. They obtain that the γ-sheet is a hole-pocket and around α instead of an electron-pocket and around β. This can be obtained in the band theory by tuning the Fermi surface closer to the van Hove singularity which this material has at 0.06 eV above the fermi energy [66]. Experimentally the ARPES measurement detected extended van Hove singularities just below the Fermi energy. The high-T_c also have these singularities and [72] compares both system.

The high-T_cs have such a high H_{c2} that no measurement of the dHvA has been achieved in them up to now. The only probe of the Fermi surface in those compound is ARPES. Since it is a surface probe there is always the possibility that it does not measure the bulk Fermi surface. In Sr_2RuO_4 both techniques can be used. If the difference between the two results is caused by surface effects in ARPES than this puts some doubts in the measurements on the high-T_c. To avoid this Yokoya *et al.* suggests a temperature dependent Fermi surface but according to Mackenzie *et al.* this should not be the case [7]. There is still no definite explanation of the difference between the two results.

The sample was obtained from Dr. A. Mackenzie at the university of Cambridge.

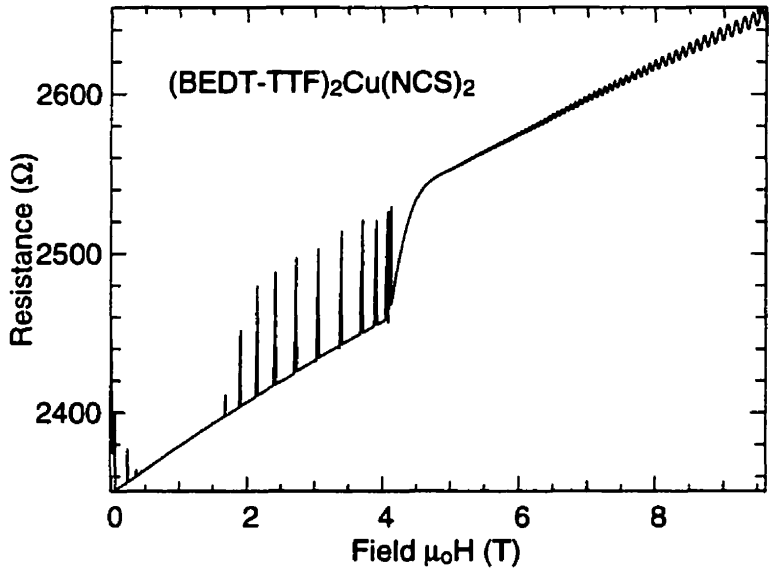

Figure 4.10: Raw data of field ramp down at 80 mK. The sweep rate is -0.075T/min for the section above 4.5 T and -0.05 T/min for the lower section.

It was grown by prof. Y. Maeno at Kyoto university using a floating-zone method [74]. It has dimensions of about 1 × 0.6 × 0.05 mm. We did not measure its T_c but other samples of the same batch were characterized by A. Mackenzie to have a critical temperature of 1 K [75]. The upper critical field of this material is less than 50 mT [69, 76].

4.4 Data and analysis

4.4.1 Organic superconductor

We begin with the data from the organic superconductor. Fig. (4.10) shows the raw data obtained during a field sweep between 0 and 10 Tesla at 80 mK. In the field range between 0 and 5 T we are in the superconducting state. The spikes are due to flux jumps. The same behavior was observed by Swanson *et al.*[50]. These occur when a local temperature instability is produced in the sample because of the power dissipated by the vortices entering or leaving the sample. These instabilities can grow catastrophically which leads to a sudden change in magnetization, a flux jump.

The upper critical field is expected to be around 5 T. Fig. (4.11) shows a blow

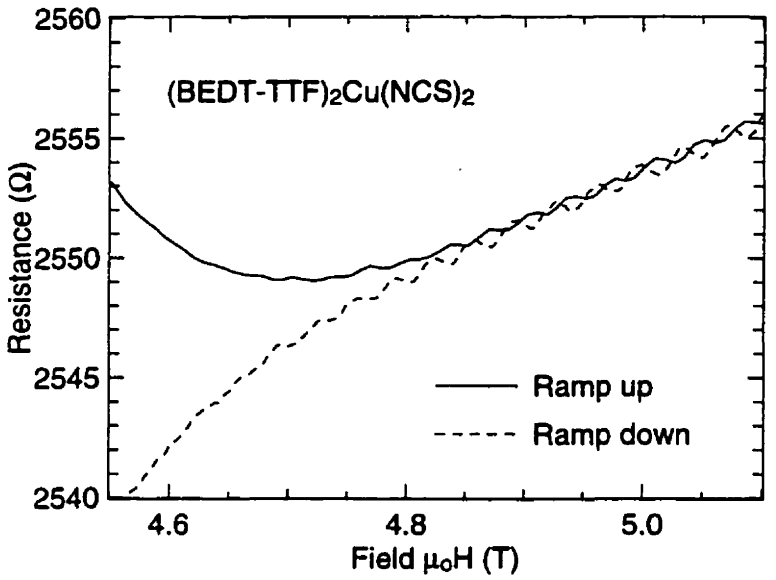

Figure 4.11: Zoom around H_{c2} of κ-(BEDT-TTF)$_2$Cu(NCS)$_2$. Both curves are at 70 mK. Ramp up at 0.2 T/min and ramp down at -0.05 T/min. H_{c2} is about 4.8 T.

up of two field sweeps around 5 T. The first one is a sweep with increasing field and the other with decreasing field. The two curves start deviating around 4.8 T. We can define that field as H_{c2}. This behavior is expected upon entry into the superconducting state since the vortices are hysteretic. This coincides with a similar observation by Swanson *et al.* [50].

To really show the periodicity, fig. (4.12) shows the signal between 5 and 10 T versus inverse field. Here we have removed the magnetoresistance background by fitting a 9^{th} order polynomial through the data. Fig. (4.13) shows the Fourier transform of fig. (4.12). That was actually calculated using a discrete Fourier transform (DFT) which requires the data to be equally spaced. The data was taken at a constant rate during the field sweep therefore the data was uniformly spaced with respect to H and not H^{-1}, as needed. To obtain the correct distribution, the data was linearly extrapolated between the points. Also, to improve the narrowness of the peak the data is multiplied by a window

$$w(x) = 1 - \left| \frac{2(x - x_o) - (x_f - x_o)}{x_f - x_o} \right| \tag{4.27}$$

where $x = 1/H$ and $xo \leq x \leq x_f$. The effect of the window is to smooth out the effect

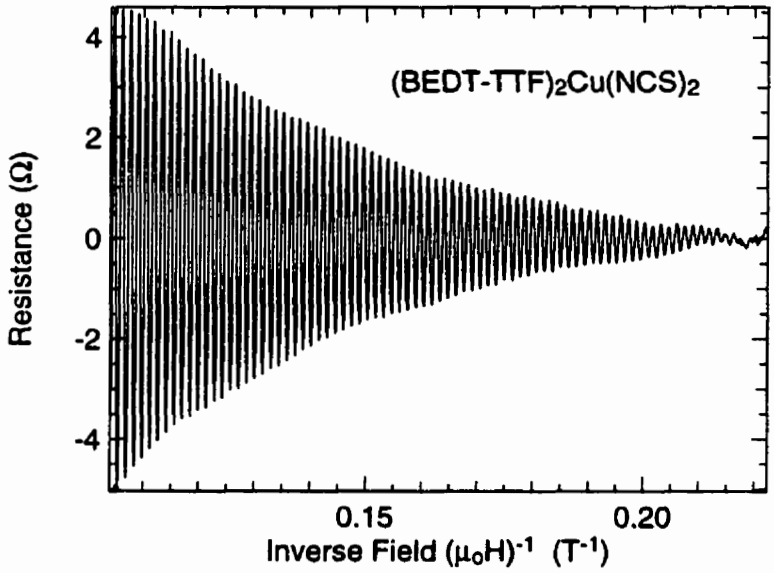

Figure 4.12: κ-(BEDT-TTF)$_2$Cu(NCS)$_2$ signal versus inverse field.

of the finite range of data used. No window is like using the raw data over a large range and multiplying it by a square window. The reason for the improvement is that if the experimental frequencies do not fall exactly on one of the discrete frequency of the DFT then its amplitude will leak into many adjacent bins. The square window is the worst in this respect. Many different windows exists. They all have different characteristics of sharpness and phase (see Numerical Recipes [77]).

We see that the signal is periodic and sinusoidal. Also only one frequency is distinguishable, as expected. The signal is also clearly above the noise level. The frequency is 691±1 T. This is to be compared to 601 T, obtained for $H \parallel a$ where a is the unit vector out of the plane [49]. Since the sample is oriented with its a axis at 30° from $\vec{H}$ we expect the frequency to be

$$F(30) = \frac{F(0)}{\cos(30)} = \frac{601}{\cos(30)} = 694. \tag{4.28}$$

Since that is what is observed we can conclude the sample is oriented as expected. This is something that needed to be checked since the sample is small and can be mounted not exactly parallel to the piezo. What is actually oriented at 30° is the sample mount which is assumed to be parallel to the piezo. Another cause of misalignment is the thermalizing wire. This wire, upon cooldown, contracts and can pull on the sample,

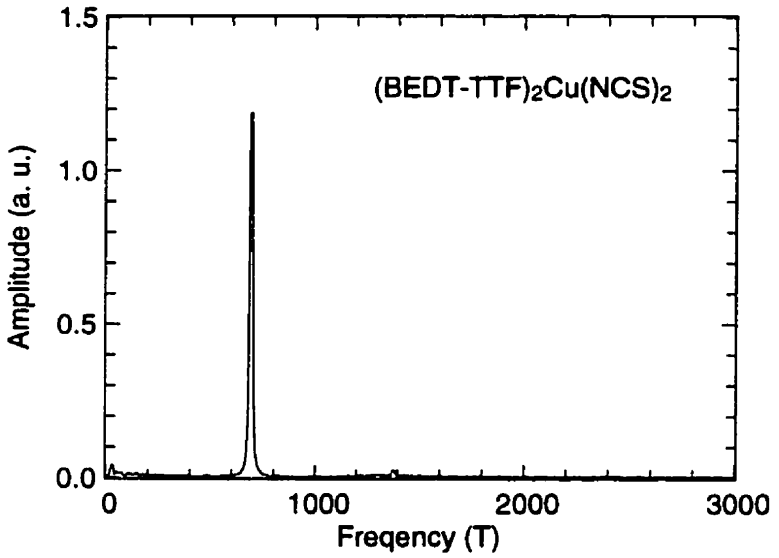

Figure 4.13: Fourier transform of κ-(BEDT-TTF)$_2$Cu(NCS)$_2$ signal. The data actually goes to 6680 T.

displacing it before the vacuum grease freezes or pulling the sample and the piezo if the spring constant is large enough. We will come back to this last point later.

To extract more information, like the effective mass and the Dingle temperature, we took field sweeps from 9.6 to 10 T at a few temperatures. We then fit every one of those with

$$R = A + BH + C \sin\left(2\pi \frac{F}{\mu_o H} + D\right). \tag{4.29}$$

where A and B are used to remove the background resistance and magnetoresistance. D is the phase shift and C the amplitude. This is a non-linear fit with 5 free parameters (A, B, C, D, F). For the fitting procedure to work, good initial guesses must be provided. For the frequency, we can use the value obtained from the DFT. We can improve the fit by keeping constant some of the parameters. The frequency F can be fixed using the frequency obtained from the Fourier transform. A better approach is the following iterative approach. We start from a fit of the LK formula to the signal between 5 and 10 T using the measured mass and Dingle temperature obtain from literature as initial guess, but leaving them as free parameters. Since for a constant temperature they are highly correlated the fit cannot extract the mass and Dingle temperature but it does give a highly accurate frequency. This is more sensitive than

the Fourier transform since here we effectively fit the oscillating signal with *one* sine wave while the Fourier transform extracts the amplitude of the signal at a discrete set of frequencies. For a field interval of 5 to 10 T the discrete frequency interval is 8.5 T.

With F fixed only four parameters are left. This can be decreased even more if we fix the phase D. This was not done since the phase actually varied slightly between runs. It varies even more between increasing and decreasing field sweeps. The theory actually says the phase should be a number independent of the field. The contradiction is resolved by understanding the measurement technique. The lock-in has a certain signal bandwidth. It was set to about 1 Hz in this case. When the field gets swept at a constant rate the field dependent oscillation gets turned into a time dependent oscillation. If this is to fast it will be filtered out by the lock-in. This filtering out decreases the amplitude and shifts the phase. The phase can be easily understood. It takes a certain time for the initial change to the signal to be translated to the output. This time lag gives the phase shift. In the experiments the field sweep rate and filter bandwidth were chosen so that the amplitude was not affected and the data was collected quickly to permit many sweeps with different excitations. These parameters still affected the phase but it did not matter since we were not interested in that value. Fig. (4.14) shows an example of this type of fit to eqn. (4.29).

Values of C thus obtained at different temperatures, using an excitation that did not show self-heating of the piezoresistance, are plotted as open squares in fig. (4.15). As can be seen the amplitude in the interval between 0.1 K and 0.8 K changes rapidly (by about a factor 10). The sample can therefore be used as a sensitive thermometer. If we know the amplitude of oscillation we can use fig. (4.15) to obtain the temperature. Of course that is assuming that the sample was actually at about the same temperature as the fridge, since the temperature axis of fig. (4.15) is the fridge temperature. This can be checked by using the temperature dependence of the LK formula. Remember that

$$R_T = \frac{x}{\sinh x} \tag{4.30}$$

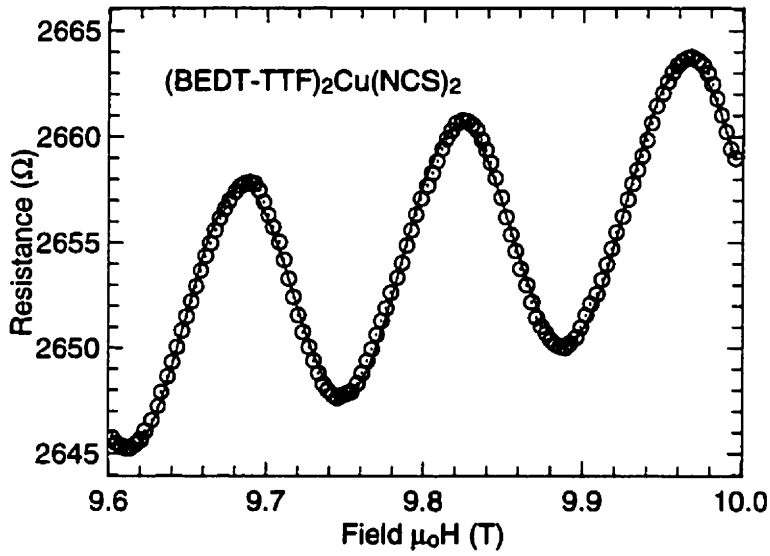

Figure 4.14: Example of amplitude fit obtained using a standard nonlinear fitting method.

where $x = 14.69\frac{pmT}{\mu_o H}$. Here we have only the first harmonic hence $p = 1$. The only other constant is m the effective mass. We know from literature that it should be around 3.2 [49] for $H \parallel a$. In our case, at 30°, we therefore expect

$$m(30) = \frac{m(0)}{\cos(30)} = 3.7 \tag{4.31}$$

To find if this is what we observed we fit fig. (4.15) with

$$C = A\frac{14.69mT/\mu_o H}{\sinh(14.69mT/\mu_o H)} \tag{4.32}$$

where A is the arbitrary amplitude at 0 K. The curve fits well trough all the points (open symbols) and gives 3.65±0.02 m_e as the effective mass. That is close enough to what is expected to believe we have a well thermalized sample.

A further check is to use smaller and larger excitations and to measure the amplitude over the same field interval. We observed no change for the smaller excitations or the slightly larger ones. With a much larger excitation the amplitude actually decreased a little signifying that the sample was warmed up. These points are shown in fig. (4.15) as black squares. From the graph we can see that the 100 mK point is really at about 150 mK meaning that the sample was warmed up by about 50 mK. This should be compared to the temperature change of the piezo which is warmed up

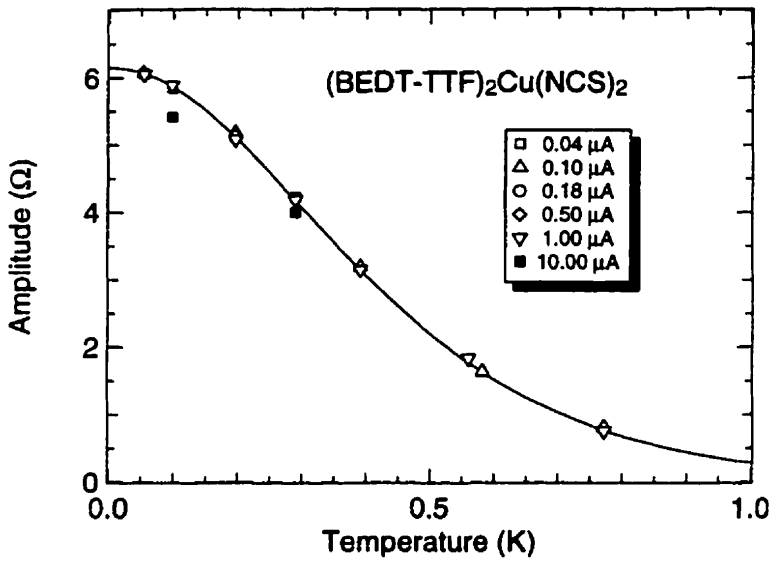

Figure 4.15: Mass plot of κ-(BEDT-TTF)$_2$Cu(NCS)$_2$. The data used for the fit are the open symbols. The errors on the amplitudes are smaller than the symbols. The filled squares are data obtained for a very large excitation and shows heating.

above 1 K. This is seen in fig. (4.16) where the base resistance of the piezo is shown as a function of the fridge temperature. The resistance is obtained from the amplitude fits (eqn. (4.29). What is actually shown is $A + 10B$ which is the resistance at 10 T. Here we assume that $\Delta R(T, H) \approx \Delta R(T, 0)$, *i.e.* that the temperature dependence of the magnetoresistance is small. If we assumed the low excitation data, the top points, to give the real curve we can see that over all the range of excitations used the resistance went down implying a higher resistance and self heating. We can see that for the very high excitation the temperature of the piezo really looks to be above 1K. Also the intermediate excitations significantly raised the piezo temperature without affecting the sample temperature. Hence the thermalizing wire is doing a good job to keep the sample cold.

Once the effective mass is known, the Dingle temperature can be extracted. No new data is needed, since T_D is obtain from a field sweep at constant temperature. That is actually what was initially obtained (fig. (4.12)). To extract it we fitted the data with the LK formula, but fixing the value of the effective mass previously

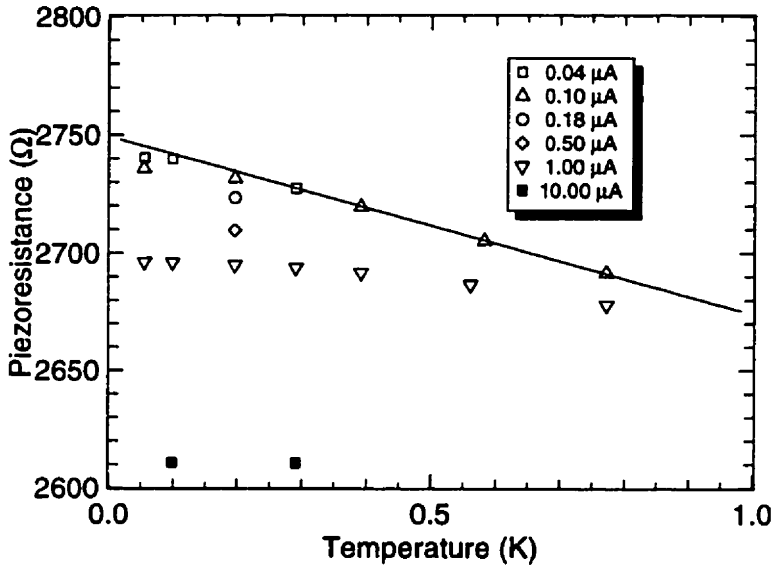

Figure 4.16: Resistance of piezo at different excitations at 10 T. The line is just to guide the high.

obtained ($m = 3.65$). Therefore, with T_d, F, ϕ, A as parameters in

$$\Delta R = A\frac{F}{H}R_T R_D \sin\left(2\pi\frac{F}{H} + \phi\right) \tag{4.33}$$

where $R_T = 14.69mT/\mu_o H \sinh(14.69mT/\mu_o H)$, as before, and

$$R_D = \exp\left(\frac{14.69pm'T_D}{\mu_o H}\right). \tag{4.34}$$

Again since we only have the first harmonic we set $p = 1$. We need to note that we have used m' instead of m. This variable is still a constant but it does not have to be the same as m since this one should not include the electron-phonon renormalization. Therefore people sometimes give the Dingle temperature as $m'T_D$. Here we follow an other convention. We set $m' = m$. The background magnetoresistance is removed before the LK fit by fitting a 6^{th} order polynomial to the data. Then a non-linear fit to eqn. (4.33) over the whole field range (5-9.6 T) is performed and we obtain T_D =0.33± 0.01K. This compares well with values reported by other people. It can be converted into a scattering rate $\Gamma = \tau^{-1} = .27$ THz or a mean free path $l = 0.15$ μm. This reflects the very good quality of samples obtain by the electrochemical growth technique.

To examine the impact of the superconducting state, we proceed by fitting the

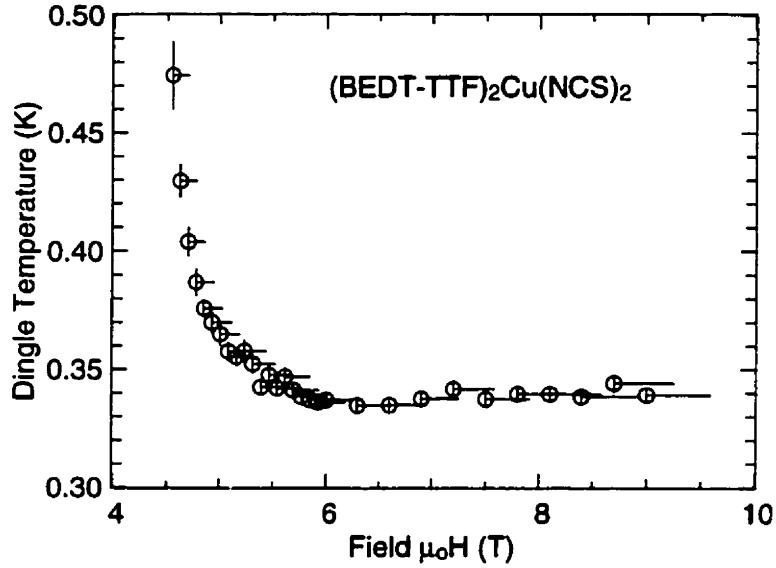

Figure 4.17: Dingle plot of κ-(BEDT-TTF)$_2$Cu(NCS)$_2$. The horizontal line shows the range (of 5 oscillations) used for each fit, the vertical one the error. The error grows at low field because the signal rapidly disappears.

LK formula over a small number of oscillations. To remove the effect of the other parameters we fix them to their value obtained during the full field range fit. Also, because on entering the superconducting state the background changes rapidly, the polynomial fit that was used to remove the background over the whole range does not do a good job there. So we choose an interval long enough to have 5 oscillations, remove the background on this short interval by a third order polynomial and fit the LK formula with only T_D as the free parameter. Following that procedure we obtain fig. (4.17). The Dingle temperature is constant in the normal state (above 5 T), as expected. Upon entering the superconducting state it suddenly increases. This has been observed in this material by P.J. van der Wel *et al.*[51], but the field range where we observe the signal in the mixed state is too small to compare it to any theory.

4.4.2 Sr_2RuO_4

We now present the same experiment on Sr_2RuO_4. The angle of the sample was set to about 25°. This time we thermalized the sample with 4 wires of about 2 cm of 12 μm copper, because this will be more flexible while carrying as much heat as a single 50 μm wire. The upper critical field in this material is 50 mT which is really low.

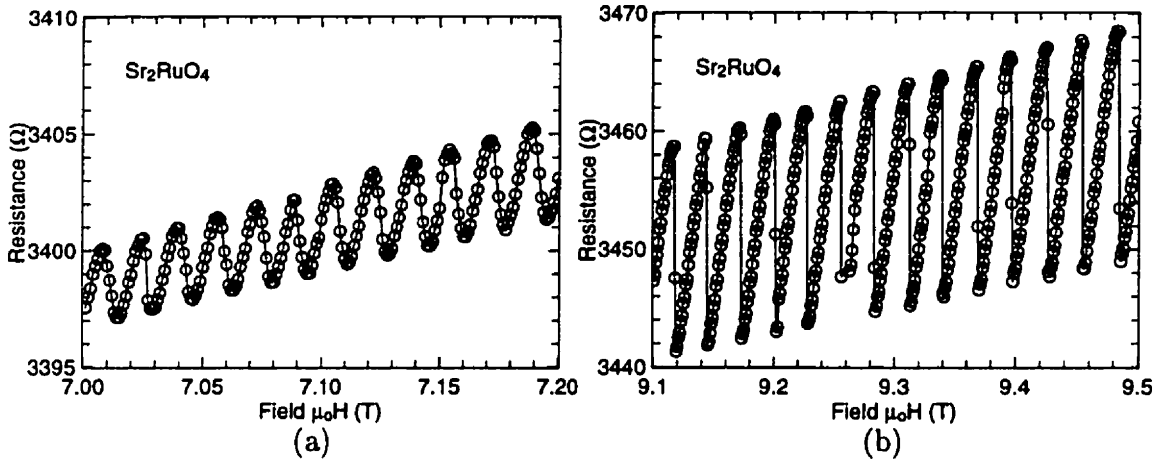

Figure 4.18: Raw data obtained for Sr_2RuO_4. (a) is for low field and (b) is for high field. The line just connects the points to help visualization.

Therefore even at low fields we did not see any signal due to the superconducting state. This is again due to the hysteresis which swamps out any signal which we could have seen below 10 mT.

Fig. (4.18) shows the raw data at 7 and 9 Tesla. It is easy to see that the signal at high fields is not sinusoidal. The waveform is now a sawtooth wave. This is also seen it the Fourier transform which is show in fig. (4.19). It shows many peaks at multiples of the fundamental which is about 3.06 kT. The next one is expected at 12.7 kT. Because of a heavier effective mass its amplitude should be smaller. But because the first harmonic is distorted so much we see a large signal at 12 kT. This makes it hard to distinguish the other signal. If we use the frequency obtained by A. Mackenzie of 3.05 kT [69] we can say that the sample is not at 25°. The angle is probably more like 10°. This small angle reduces the amplitude of the signals and therefore we have only observed the first fundamental frequency.

The shape of the signal can be expected if we were at 0 K and if there were no impurity scattering as explained in the theory. But this is not the case here. The

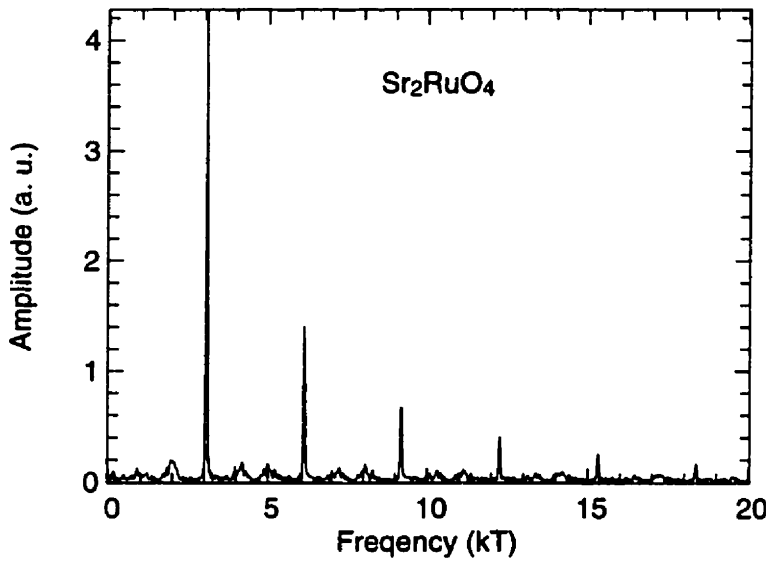

Figure 4.19: Fourier transform of Sr_2RuO_4 signal.

shape is due to torque interaction (TI). We explain TI by writing the signal as

$$\tau = a\sin\left(2\pi\frac{F(\theta)}{\mu_o H}\right) \approx a\sin\left(2\pi\frac{F(\theta_o)}{\mu_o H} + \frac{2\pi}{\mu_o H}\frac{\partial F}{\partial\theta}\delta\theta\right) \tag{4.35}$$

where θ is the angle of the field with respect to the a axis of the sample, a is a constant, and $\delta\theta = \theta - \theta_o = b\tau$ where b is another constant. This is because we measure the torque by measuring the motion of the piezo. This motion corresponds to a change in angle. Therefore as the magnetization oscillates, this makes the angle oscillate, which in turn changes the magnetization. To simplify eqn. (4.35) can be recast as

$$\tau = a\sin\left(2\pi\frac{F(\theta_o)}{\mu_o H} + 2\pi c\tau\right) \tag{4.36}$$

where $c = \frac{b}{\mu_o H}\frac{\partial F}{\partial\theta}$. This equation is displayed in fig. (4.20) with $x = 2\pi F/\mu_o H$, $y = 2\pi c\tau$ and $2 = a/2\pi c$. The effect of b or c is to shift the curve proportionally to the amplitude of the signal. This slants the sine waves. When the signal gets this much distorted, it is no more single valued. Therefore the system will jump to the point with the lowest free energy. When this occurs you obtain a straight line and the signal looks like a sawtooth. The additional phase $2\pi c\tau$ oscillates by an amount of $2\pi ca$. Therefore the condition that makes TI not important is $ca \ll 1$. For this sample we have at $\mu_o H = 8.3$ T, $a = 6\ \Omega$, $c = b\frac{F}{H}\frac{1}{F}\frac{\partial F}{\partial\theta}$ where $\frac{1}{F}\frac{\partial F}{\partial\theta} = \tan(\theta)$ for a 2D

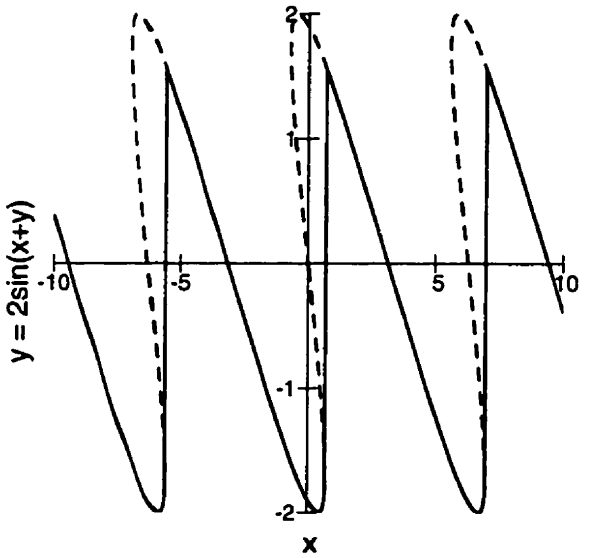

Figure 4.20: Sketch of torque interaction. The dash line shows the multivalued torque. The solid lines shows the actual observed signal for an increasing magnetic field.

system and $b = 8 \times 10^{-4}$ rad/Ω. At this field the signal is starting to have the straight line which means it is close to $ca = 0.25$. Using an angle of about 10°, $F = 3.06kT$ we calculate $ca = 0.31$, which is just the right size to explain the observed signal. Hence the sawtooth is really caused by a TI problem.

To obtain a precise value of the frequency we fit the LK formula between 7 and 10 T. We obtain 3.06±0.01 kT. Again we mention that comparing our result to the work of A. Mackenzie [69] we find that the angle of the sample is probably around 10°. This is also to be expected since the base resistance of the piezo is 3.2 kΩ instead of the usual 2.5 kΩ. This implies that the thermalizing wire is pulling down on the sample.

We can carry the same analysis that was done on the organic superconductor on this sample, but we expect the fits to become worst and worst as the field increases, because the data is less and less sinusoidal. Fig. (4.21) shows the mass plot and the low temperature data have larger errors. This is because the larger the amplitude the more TI there is. The mass which is obtained is 3.1±0.1 m_e. But since at low temperature the signal is more sawtooth like, the sinusoidal fit will under evaluate the amplitude so we can assume that the real amplitude can be bigger. This would

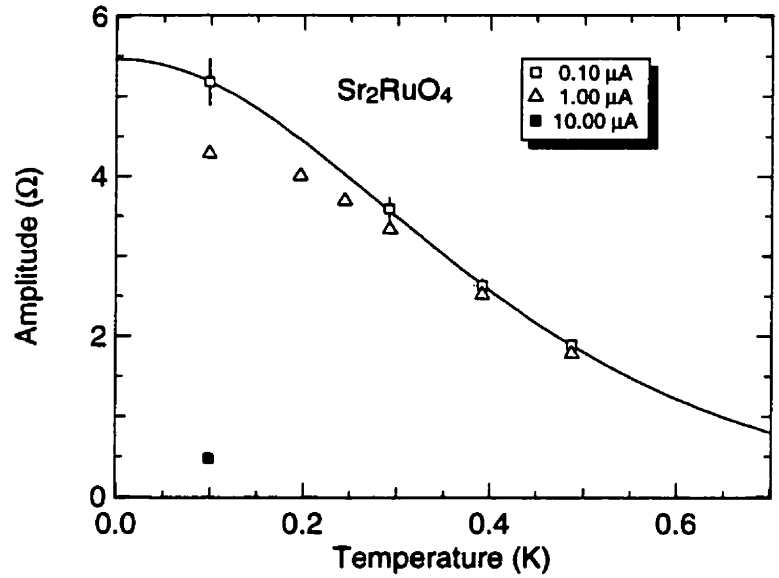

Figure 4.21: Effective mass of Sr_2RuO_4. The vertical lines show the error on the data used for the fit to $14.69mT/\mu_o H \sinh(14.69mT/\mu_o H)$.

give a larger mass and bring us closer to 3.4 m_e measured by Mackenzie [69].

Also, we see that with the same maximum excitation as for the organic we get more heating of the sample in this case. Therefore the thermal contact between the sample and the fridge was not as good as before. This can be due to the silver paint which did not make a good thermal contact between the small wires and the sample. It can also be that the small wires were partially broken while the sample was mounted. Finally the small wires were difficult to solder to the sample mount.

A final point to the analysis. We can try to extract the Dingle temperature. We obtain about 0.59±0.03 K (which means l_o = 0.21 μm) which compares very well with the measurement of Mackenzie of 0.59 K [69]. It is constant over the explored field range.

4.5 *Problems and solutions*

The experiments on Sr_2RuO_4 showed us some problems with this experimental technique. While it certainly can work as was shown by the organic superconductor experiment, it can be plagued by torque interaction and an improper thermalization.

The torque interaction can be attenuated by having a stiffer cantilever. But, just making the spring constant bigger will decrease the sensitivity. A better way is to use a feedback mechanism to keep the angle constant, this provides a higher effective spring constant without losing sensitivity. A possible way to do this is to add a capacitor plate very close to the sample and use the sample as the other plate. By changing the voltage between sample and plate, the electrostatic force can be used to compensate the magnetic torque.

To prevent the improper thermalization a better way to make a good contact is needed. The smaller wires (12 μm diameter) are harder to use and therefore the risk of a bad contact is greater, while the larger wire (50 μm) as been shown to work. Therefore the larger wire should be used. The problem can also have been caused by the silver paint. To fix this we should use silver epoxy, which we have used successfully to make thermalconductivity contacts on $YBa_2Cu_3O_{7-\delta}$ samples for low temperature measurements.

To map the Fermi surface of metals, the dHvA frequency for different orientations of the crystal is needed. So to really use this system we need to have a rotation mechanism that allows us to rotate the sample in situ. This can be achieved by a mechanical feedthrough, or using a cold steeping motor.

5

LOWER CRITICAL FIELD

5.1 Magnetization measurement by torque

We are interested in the lower critical field (H_{c1}) of superconductors. This can be obtained by measuring the magnetization of a sample at low field. H_{c1} is defined as the field where the magnetization deviates from linearity. To measure the magnetization using torque we need some anisotropy. In this case it comes from the sample shape.

If we assume the sample is an ellipsoid then we have that the field $\vec{H}$ inside is uniform. It is related to the applied field, $\vec{H}_a$, by a demagnetizing coefficient n which is a tensor. Assuming the field is along the principal axis of the ellipsoid then we only have three parameters, n_{xx}, n_{yy}, n_{zz}. We will write them as n_x, etc. Also $n_x + n_y + n_z = 1$ and

$$n_i = \frac{l_x l_y l_z}{2} \int_0^\infty \frac{ds}{(s + l_i^2)\sqrt{(s + l_x^2)(s + l_y^2)(s + l_z^2)}} \tag{5.1}$$

where l_x, l_y, l_z are the semi axes of the ellipsoid along x, y and z and i can be any of x, y, z. Therefore the ellipsoid volume is $\frac{4\pi}{3} l_x l_y l_z$. With these n's we write

$$H_{ai} = H_i - H_i^{\text{demag}} = H_i + n_i M_i \tag{5.2}$$

where M is the magnetization[1]. Combining this with

$$H_i = \frac{B_i}{\mu_o} - M_i \tag{5.3}$$

[1] $\vec{M}$ and $\vec{H}$ come from the microscopic distinction between bound and free currents. This distinction is not applicable to a superconductor since they both have the same physical origin. Nevertheless we keep them as useful tools. In the discussion above we assume the superconductor only contains bound currents.

we obtain

$$H_{ai} = \frac{n_i B_i}{\mu_o} + (1 - n_i) H_i. \tag{5.4}$$

Inside a superconductor $B_i = 0$, so we can write

$$M_i = -H_i = -\frac{H_{ai}}{1 - n_i}. \tag{5.5}$$

Using it we can calculate the change in free energy due to the magnetic field:

$$\Delta \mathcal{G} = -\int_{\text{Volume}} \int_0^{H_{ai}} \mu_o \vec{M} \cdot d\vec{H}_a d^3x = V \sum_i \frac{\mu_o H_{ai}^2}{2(1 - n_i)} \tag{5.6}$$

where V is the volume of the sample. Lets pick $\vec{H}_a$ as $H_{ax} = H\cos\theta$, $H_{az} = H\sin\theta$ and $H_{ay} = 0$ then

$$\Delta \mathcal{G} = \mu_o V \frac{H^2}{2} \left[\frac{\cos^2\theta}{1 - n_x} + \frac{\sin^2\theta}{1 - n_z} \right] \tag{5.7}$$

where H is the amplitude of the applied field. The torque τ is finally obtained by:

$$\tau = -\frac{d\Delta \mathcal{G}}{d\theta} = \frac{\mu_o H^2}{2} \sin(2\theta) \left[\frac{1}{1 - n_x} - \frac{1}{1 - n_z} \right]. \tag{5.8}$$

From this equation it is easy to see, as expected, that the torque will be zero when the field is aligned along the principal axis of the ellipsoid. It will also be zero if the ellipsoid is a sphere since then all the $n_i = 1/3$.

Assuming the magnetization deviates from its linear law at $\vec{H}_a = \vec{H}_o$ then the critical field is

$$H_{c1x} = \frac{H_{ox}}{1 - n_x} \quad \text{or} \quad H_{c1z} = \frac{H_{oz}}{1 - n_z}. \tag{5.9}$$

To distinguish between the two the angle can be changed. If the angle is close to 0° then you measure H_{c1x}. If the angle is close to 90° you measure H_{c1z}

When a type I superconductor has $H_a < H_c$ but that the calculated H from demagnetization is above the critical field, an intermediate state is entered [29]. In this state, alternating layers of normal and superconducting regions organize so that $H \leq H_c$. This as to be the case since if the sample is fully superconducting the field inside is larger than H_c which is inconsistent. Similarly if the sample is all normal than H is less than H_c and it should be superconducting. So the sample enters the intermediate state with both normal and superconducting regions. But this is not

the mixed state of a type II superconductor. It occurs only in type I superconductors because of geometry. To prevent this the demagnetizing factor should be small so that $H_a \approx H$.

In a type II superconductor this is not a problem but deviations from a perfect ellipsoid, such as having a sample with corners, will produce a non-uniform H field inside the superconductor. Since H will tend to be larger at the corners, vortices will enter there before the value predicted using the approximate demagnetization coefficients. This will make the measured H_{c1} lower than the value of the bulk. To prevent this the sample shape should be made as close to an ellipsoid as possible or with a geometry that makes $H_a \approx H$, such as a wire.

5.2 Experimental technique

Here we describe the experimental technique that was used to measure H_{c1} of $YBa_2Cu_3O_{6.9}$.

5.2.1 Dipper

Since $YBa_2Cu_3O_{6.9}$ is a high-T_c compound with a T_c of 91 K, the dilution refrigerator is not needed to observe the superconductive phase. Therefore we used a simpler system. We call it a dipper (RMC model 4HeIC) and it is shown in fig. (5.1). This is designed so that it can be inserted directly inside a helium storage dewar. When it is immersed in liquid, a minimum temperature of 1.3 K can be reach by pumping on the 1 K pot inside. The temperature is controlled with a Lakeshore DRC-93CA temperature controller which reads either a platinum thermometer (from 30 K to room T) or a germanium thermometer (from 1 to 60 K). Outside of their range the thermometers loose sensitivity. The heater consists of a 50 Ω resistance made of manganin wire. The temperature controller can deliver up to 50 W but to help it at higher temperatures we raise the can above the liquid into the helium gas. It can also be used in a liquid nitrogen container in the same way.

Fig. (5.1) shows the inside of the dipper can. The 1 K pot is currently used in one-shot mode. To use it we liquefy helium in it by applying an overpressure of He

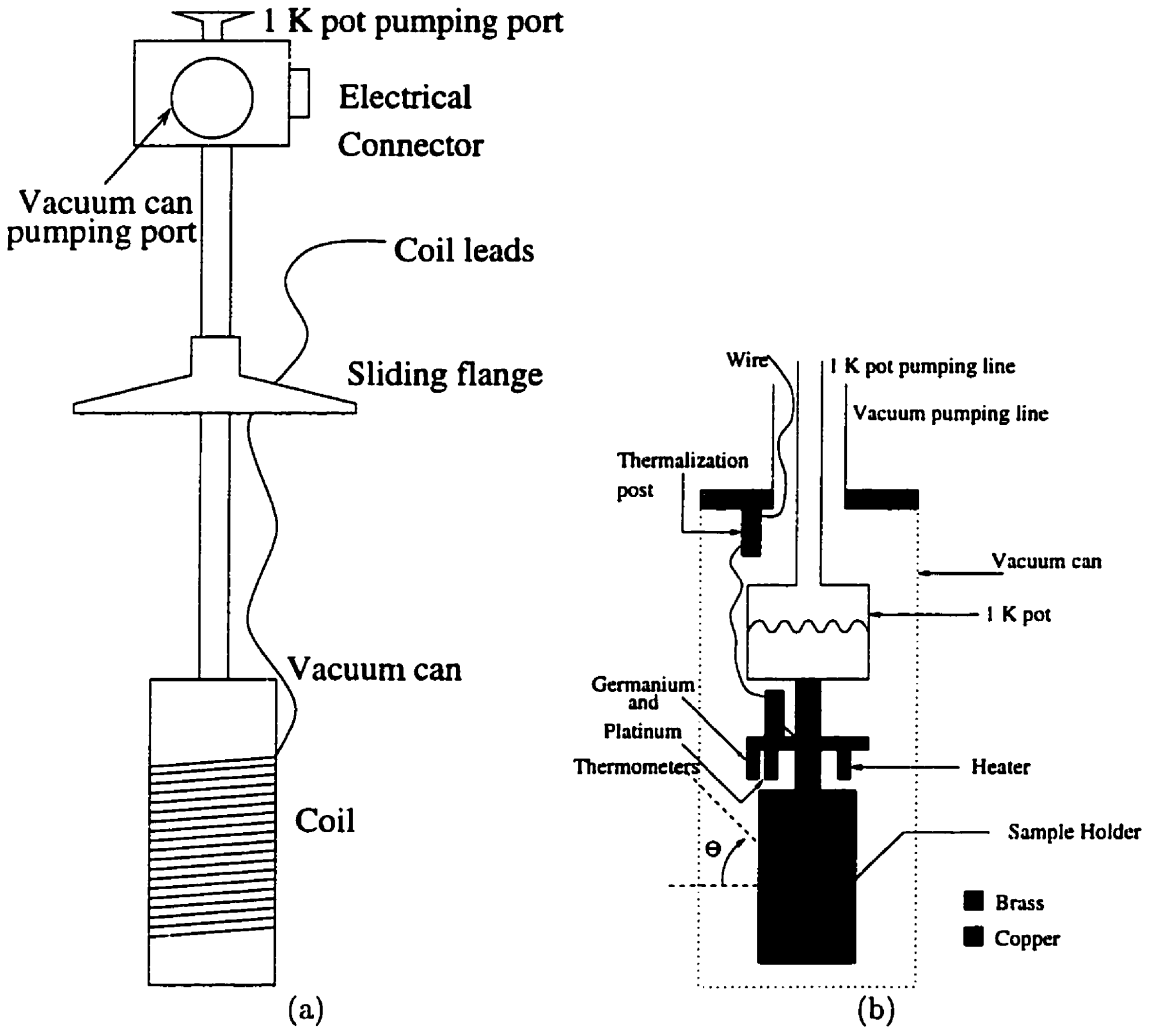

Figure 5.1: Schematic of the dipper. (a) shows the dipper with the sliding flange and the home made coil and (b) shows the inside of the vacuum can.

gas from outside. This is done once the can is immersed in liquid helium. To help the liquefaction we leave a small pressure of He gas in the can to act as exchange gas. Once the liquefaction stops because the pot is filled, we pump out the exchange gas very well. After that we can start pumping on the 1K pot and it cools down to about 1.3K. The copper plate containing the thermometers, heater and which is connected to the copper sample holder is separated from the pot by a brass tube. Copper is a very good thermal conductor so it is all well thermalized at a single temperature. The brass tube acts as a weak thermal link through which heat can be extracted but it can sustain a good thermal gradient. Hence the pot can be at a certain temperature, the

copper at another and the difference will appear across the brass and not in the Cu. So we assume that all the copper is at a single temperature. The advantage of the weak link is that the heater only needs to change the temperature of the copper. It does not have to warm up the liquid helium in the pot which would require a lot more power and shorten the duration of the pot. It usually lasts about an hour. After that the cycle can be restarted. The pot could also be used in continuous mode by adding an intake tube through a flow impedance. The cooldown procedure takes from one to two hours.

To limit the loss of heat through the wires these are thermalized on top of the can, which is usually at 4.2 K. They also get thermalized on the Cu plate so that the wires going to the experiment or to the thermometers are already at the correct temperature. What limits the minimum temperature is the pumping speed achievable and the heat load on the lower stage. I rewired the dipper because it was using mostly copper wires which had too good a thermal conductance and they were shorting out the brass weak link. I replaced them with manganin wire which can have a larger diameter, and therefore easier to manage, and still have a smaller thermal conductance than copper. We also have 2 coaxial cables installed for ultrasound experiments. The lowest temperatures were not needed in most of my experiment but they are used for thermal conductivity measurements. It is also close to the upper limit of the dilution fridge which is about 1.2 K. Therefore with the two cryostats we can span almost continuously the range between 50 mK and room temperature.

5.2.2 Coil and electronics

For our experiments we need a field that will reach H_{c1}. In the material of interest it is of the order of 20 mT. Therefore we need a magnet that can provide such a field and that can fit within the experimental setup we already have. It also needs to work in the temperature range of 4-100 K. The solution we employed was to use a copper coil that slips on just outside the vacuum can as shown in fig. (5.1). Of course it cannot be too thick otherwise it will not be insertable into the storage dewar. As for the length we made it equal to the diameter so that the field at the center is

approximately that given by an infinite solenoid. The field at the ends is then about $1/\sqrt{2}$ that of the middle which gives a small field gradient in the middle. A longer magnet lowers the gradient but will not increase the field inside, and could add a lot of wire. Since we use copper, we have some resistance which will dissipate power in the liquid helium so the shorter the length we have the better. With 1 W of power we loose about 1L/hour of liquid helium. This is as much as we would like to loose (the dewars have 100 L).

The limited volume of the coil, the choice of copper and the limit of power actually defines the maximum field attainable. This maximum is independent of wire diameter. Since copper is the best conductor, after silver, we can only improve on this by using superconducting wire. But it is more expensive and when the wire is not in liquid helium and cooled enough it will be resistive. To choose the wire size we decided that the maximum current we could supply is 1 A. With that choice the wire has to be 30 AWG (0.25 mm diameter). With that wire we made the coil. It has a diameter and length of 5 cm, it contains 13 layers each of 168 turns of the 30 AWG wire. It has a resistance of 100 Ω at room temperature and of about 1 Ω at liquid helium temperature. Therefore it does dissipate about 1 W at maximum current. At that maximum current the field in the center is 36 mT. This calibration was calculated from the the geometry and checked with a gaussmeter to be valid within 10%. Finally the coil has an inductance of about 0.1 Henry.

It is powered using the circuit of fig. (5.2). The current is controlled by the 1 Ω limiting resistor (R_2). By reading the voltage across the 1 Ω resistor (R_1) we know the current that passes through the coil. Since a 1 Ω resistor with 1 A dissipates 1 W, it can easily warm up. This could change its resistance. To prevent this increase in temperature we use high power resistances (100 W) that can dissipate the energy without heating up. The power supply can actually deliver 15 A and has a limit of 20 Volts. The circuit is designed so that with a 10 V input we obtain 1 A and that with a 5 V_{RMS} input we also obtain 1 A peak. The lock-in we use has auxiliary outputs that can supply DC voltage between -10 and +10 Volts and a sinusoidal reference up

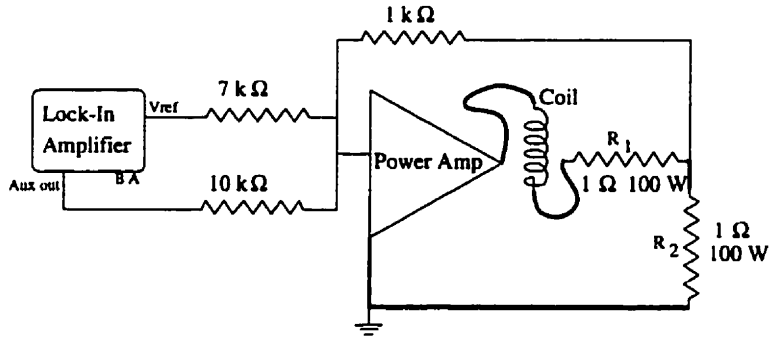

Figure 5.2: Current supply of home made magnet.

to 5 V_{RMS}.

5.2.3 *Measurement electronics*

The measurement can be done using the same circuit as for the dHvA experiments. We will refer to that configuration as the DC technique. Another possibility is to oscillate the field. This is done by controlling the current in the coil using the reference output of another lock-in. Therefore we use a similar circuit as before to measure the resistance, with a high frequency (700 Hz). We obtain a resistance which will oscillate at a harmonic of the field modulation frequency, chosen to be small (.5-5Hz) in order to limit eddy current heating. We use the analog output of the X component (in phase) of the first lock-in and use it as the input to the second one, the one which modulates the field. With this last lock-in we can detect the resistivity oscillations amplitude at any harmonic we like. We will be mostly interested in the second and fourth. Fig. (5.3) shows this circuit.

For the second lock-in to detect anything, the first one must let through the low frequency signal. Therefore its filter bandwidth must be chosen large enough that the desired signal can pass. But with a filter bandwidth too large, noise can overload the output. Therefore a comprise must be reached. Usually the observed amplitude is attenuated by a factor of 10% and the phase can be shifted by as much as 150°. The large phase shift is because the filter is a 4 pole filter. It has a faster frequency curve but worse phase characteristic. This phase shift and amplitude attenuation only depend on the operating frequency and filter time constant and can therefore be

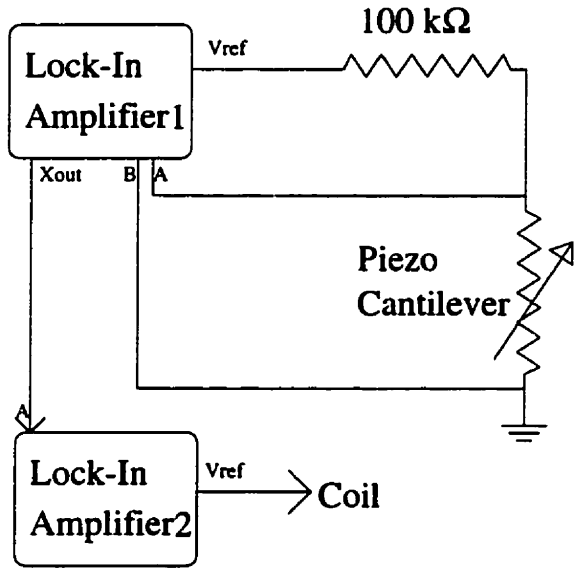

Figure 5.3: Diagram of setup for the modulation measurement.

calculated. Hence the data can be corrected for these factors. For a given experiment they are constants which do not change.

Finally a word about the sensitivity. In the 20 to 100 K range we used the maximum excitation available from the lock-in and using a 100 kΩ limiting resistor. This is 50 μA_{RMS}. With the modulation technique the noise is then of 1 mΩ (which is 1Å, 0.4 ppm or 1×10^{-3} Nm).

5.3 Samples

For the experiments of this chapter we used $YBa_2Cu_3O_{6.9}$, which is a high-T_c superconductor. For more information on this class of superconductors we refer the reader to the book by Burns [78], to articles in a special issue of Physics Today [79] and to the series of volumes from Ginsberg [80].

All of the high-T_cs have one or more CuO_2 planes. This is where superconductivity is believed to occur. They have critical temperatures now reaching 150 K. They have different anisotropy. Compounds like $Bi_2Sr_2CaCu_2O_8$ (BSCCO) are very anisotropic. The interlayer coupling is very small. In fact using a sticky tape, a few layers can be removed, leaving a clean surface. This ability makes this material very good for

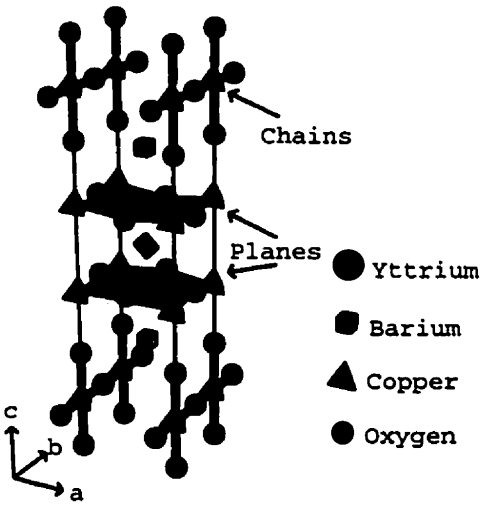

Figure 5.4: Crystal structure of $YBa_2Cu_3O_7$.

surface studies since very clean surfaces are obtained easily.

As mentioned before the high-T_c we studied was $YBa_2Cu_3O_{6.9}$. This material does not have a large anisotropy. For example the temperature dependent ratio of resistivity in the planes to the resistivity perpendicular to the planes varies from 75 to 125 while compounds of the BSCCO family have their resistivity ratio range from 500 to about 10^6. The oxygen content is set to 6.9 since that is where the maximum T_c is observed. Like in some other high-T_c compounds, superconductivity is obtained only in a certain range of doping. Here the doping is obtained by modifying the oxygen content. If we write $YBa_2Cu_3O_{7-\delta}$ then for $0.7 < \delta < 1$ we have an insulator which is antiferromagnetic. Its crystal structure is tetragonal. This proximity to antiferromagnetism exists in many other high-T_c. For $0 < \delta < 0.7$ the material is metallic and the superconducting T_c has a maximum for $\delta = 0.1$ of 93K. This phase as an orthorhombic crystal structure with a=3.86 Å, b=3.92 Å and c=11.63 Å. The CuO_2 planes are in the ab plane (see fig. (5.4)). This orthorhombicity is caused by the appearance of a new structure, called the CuO chains, along b. This is unique to this compound. The other high-T_cs do not have such a quasi one-dimensional structure.

These chains lead to an anisotropy of the resistivity in the plane, $\rho_a/\rho_a = 2.2$ [81]. Some recent data on thermalconductivity[82] and microwave measurements of the conductivity in the superconducting state of ultra-pure crystals grown in $BaZrO_3$ (BZO) crucibles [83] seem to show that there is an increase of superfluid density, possibly due to the chains, starting around 65 K. Other microwave experiments have been done before and did not observe this probably because the surface was not of good quality. The new BZO crucibles produce crystals with very good surfaces. For example the vortices have been observed by an STM without surface preparation which is not possible on standard samples (see references in [83]. The thermalconductivity measurement was done on crystals grown using the standard yttria-stabilized zirconia (YSZ) crucibles, but it is a bulk measurement and is not sensitive to the surface quality. Our interest in H_{c1} for this material is to see if the same effect could be observed in this parameter too, by looking at the anisotropy of the critical field in the plane. For this a good reproducible technique to measure H_{c1} must be developed. The standard technique of measuring the magnetization and detecting the deviation from linearity depends on fitting the low field behavior and observing departure from this field at higher field. Here we propose what we think is a more direct measurement of H_{c1}.

The previous H_{c1} data (see [84, 85] and reference therein) shows a wide range in critical fields. The zero temperature H_{c1} perpendicular to the planes ranges from 40 to 800 mT and parallel to the plane it ranges from 7 to 60 mT. The temperature dependence also varies from one experiment to another. The experiment by Umezawa *et al.*[85] indicates that the twin boundaries seem to increase the critical field of the plane. The experiment of Liang *et al.* [84] was done on an ellipsoid-shaped sample to prevent the problem of corners for the field perpendicular to the planes direction. Because a rectangular shaped sample does not have a well defined demagnetizing factor, the vortices can penetrate first at the corners. This would lower the measured H_{c1} while surface barriers to the penetration of vortices can raise the measured H_{c1}. Also the strong pinning in this material prevents flux from entering and exiting freely

from the sample at low temperature which makes the deviation from linearity of the magnetization weaker and therefore harder to measure accurately.

The crystals were grown by R. Gagnon using a self-flux method (see references in [81]), starting with powders of Y_2O_3 (99.9999%), $BaCO_3$ (99.999%) and CuO (99.9999%) mixed in a molar ratio of 1:18:45. The crystals were grown in YSZ crucibles as they are known to contaminate the crystals very weakly. Thin platelets with the c axis of the crystal along the thickness of the platelet are obtained. The crystals have dimensions of the order of $1\times1\times0.1$ mm. Because they are grown in air the crystals are not fully oxygenated. To insure optimal doping the crystals were oxygenated for 6 days at 500°C in flowing oxygen gas at a pressure of 1 bar and quenched at room temperature. Since at low oxygen content the material is tetragonal and that at higher oxygen content it becomes slightly orthorhombic, the above procedure produces crystals which are twinned. This means that domains with the a and b crystal axis rotated by 90° from one another appear in the sample. This reduces the stress in the crystal produced during the growth, but to measure the anisotropy in the plane between a and b we require detwinned crystals. The detwinning is achieved by applying a uniaxial pressure of approximately 50 MPa at 550°C in air for less than 30 minutes. Detwinned crystals are then reoxygenated for one day at 500°C. Table (5.1) list the characteristics of the samples we used. We use three $YBa_2Cu_3O_{6.9}$ samples, all with a T_c of 93 K, and a $Nb_{0.52}Ti_{0.48}$ wire. Only one YBCO was detwinned, and it was measured only along b. The circular shape was obtained by sanding away the corners using a fine sandpaper (3 μm). The angles given are for the sample mount itself. The sample could be at at slightly smaller angle.

5.4 *Data and analysis*

We begin by showing the result of a DC torque measurement. Fig. (5.5) shows a hysteresis curve obtained by measuring the piezoresistive signal as the field is first increased from 0 to 36 mT then lowered to -36 mT and finally brought back to 0.

sample name	shape	dimensions (mm)	volume (10^{-3}mm^3)	orientation	n_{ab}	n_c	n_f	angle (°)
TW1	circle plate	0.71dia×0.05	20	twinned	0.05	0.90	8.8	85
TW2	square plate	0.4×0.4×0.03	4.8	twinned	0.05	0.89	8.2	80
DTW	square plate	0.25×0.25×0.08	5.0	detwinned, b-axis	0.18	0.65	1.6	87
NbTi	wire	0.04dia×0.8	1.3	$Ni_{0.52}Ti_{0.48}$	0.01	0.5	0.97	85

Table 5.1: List of the samples used in the modulation technique. The dimensions are only approximate. They were measured with a caliper and by comparison to wires of small diameter. $n_f = 1/(1-n_c) - 1/(1-n_{ab})$ is the estimated demagnetization factor by assuming an ellipsoidal sample with the axis given by the numbers in the dimension column. The angle is between the field and the normal to the plane and is very approximate.

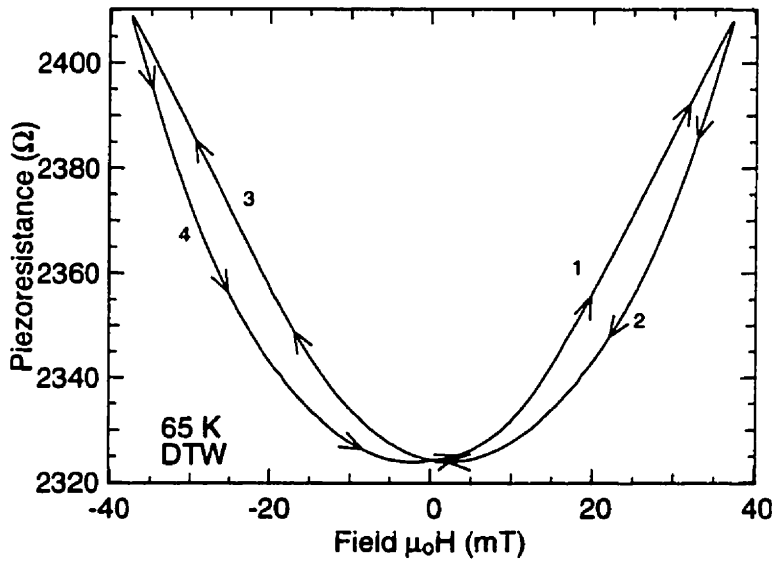

Figure 5.5: DC hysteresis torque curve taken on the detwinned sample at 65 K. The arrows show the sequence of fields.

The hysteresis is due to trapped flux in the sample, which implies we went above H_{c1}. The signal is quadratic at low field which is what is expected for the Meissner state. The start of the deviation from this quadratic behavior would give H_{c1}, but it is very hard to extract from that curve. Temperature drifts for example can shift the curve slightly up and down producing deviations from quadradicity. Also the curve depends on the previous history of the sample. After two similar field sweeps the curve will repeat but the initial run will depend on the amount of trapped flux inside.

Since the DC method is not sensitive enough we now use the modulation technique. This has the advantage that the temperature drifts are eliminated from the signal since the technique effectively just measure changes in resistance over a short cycle of about 1 s, and we average many such cycles. This enables us to use the technique to measure the T_c of very small samples of superconductors by looking at the amplitude of the second harmonic. This is because the signal is quadratic, so if the field is given by $H_o + H\sin(\omega t)$ then

$$\tau \propto (H_o + H\sin(\omega t))^2 = H_o^2 + \frac{H^2}{2} + 2H_oH\sin(\omega t) - \frac{H^2}{2}\cos(2\omega t) \qquad (5.10)$$

where H_o is a DC field and H is the amplitude of the oscillating field. In the experiments described here we do not put a DC field but there still is a small field due to the earth's magnetic field (about 0.05 mT) and there could be a field due to a material which spontaneously magnetizes at low temperature. The dewar and the dipper were constructed of materials which do not become ferromagnetic so this should not be a problem. The DC field can be seen by looking at the zeroth (DC) and at the first harmonic of the modulation frequency. Since the lock-ins are AC coupled, the DC signal is filtered out. The first harmonic is usually small, but if a large amount of flux is trapped it can give a good signal at low field. But as the modulation amplitude is increased there is a tendency to bring this first harmonic signal to zero. Therefore most of the signal is contained in the second harmonic of the modulation field frequency. Fig. (5.6) shows an example of this. It gives T_c of a small $Nb_{0.52}Ti_{0.48}$ wire to be 9 K which is compatible with previous data [86]. The second harmonic is observed while the field modulation is kept constant at 2 mT. Then the temperature is ramped slowly (0.6 K/min). When the signal goes to zero the sample is normal. The transition is sharp and has no hysteresis whether the temperature is increasing or decreasing. The transition does not move either if we lower the excitation current of the cantilever. This shows that we are not heating the sample. The excitation current was 10 μA. A higher current at this temperature of 10 K starts warming up the piezo, but above 20 K we use 50 μA without any observable self-heating. The noise of 5 mΩ (5 Å) on fig. (5.6) is because of the smaller excitation current and the

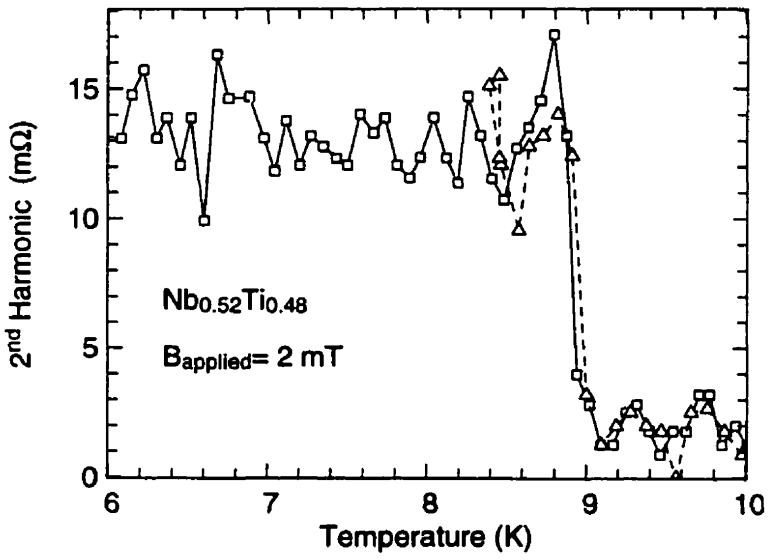

Figure 5.6: Critical temperature of a $Nb_{0.52}Ti_{0.48}$ wire. The squares (□) were obtain for increasing temperature and the triangles (△) for decreasing temperature.

small signal to noise ratio is because the sample and the field are small. The field is chosen small so that the transition is not broaden by the applied field. The signal does not go negative because we show the amplitude, *i.e.* $\sqrt{v_x^2 + v_y^2}$ where v_x is the in phase and v_y is the out of phase components obtained from the lock-in. This is the same experiment that was performed to obtain the sensitivity curve of Chapter 2 fig. (2.4), using $YBa_2Cu_3O_{6.9}$ (T_c=93 K). In that figure we plot the amplitude of the second harmonic divided by the R_o of the cantilever and is normalized to 1 at 80 K. It is important to divide by R_o since the resistance of the device changes as a function of temperature and the sensitivity of the device is expressed in terms of $\Delta R/R_o$ and not in terms of ΔR. The changes can only be due to the sensitivity of the device since the amplitude of the modulation is chosen to be less than H_{c1}. So the amplitude of the signal only depends on the geometry of the sample if we neglect the effect of the field penetration depth. This is justified since over this temperature range it changes by 0.2μm [83] which could at most give a change of 1% in the sensitivity.

When we cross H_{c1}, the signal will no be purely quadratic anymore. Therefore higher harmonics should appear. Because the original torque signal is at 2ω, distortions appear at harmonic of this frequency. So the first harmonic with a signal

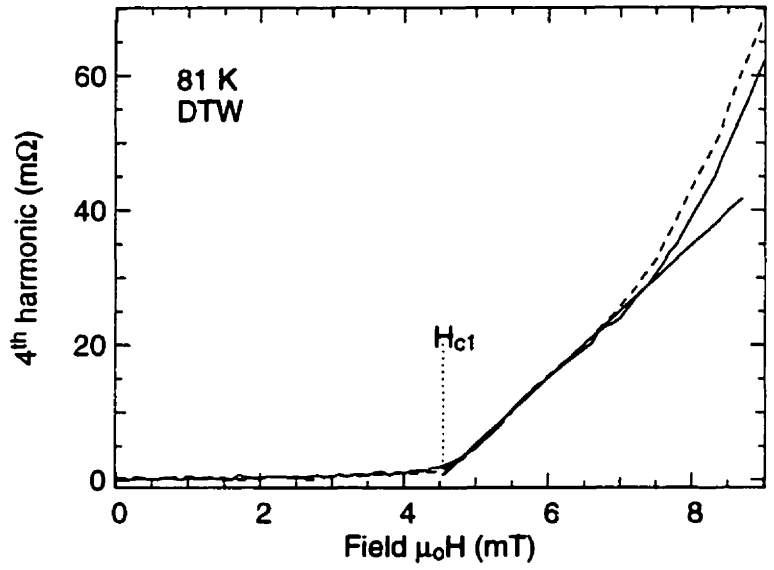

Figure 5.7: Comparison of zero and non-zero field cooled. The lower critical field can be estimated by drawing a line through the first deviating points and taking the intersection with 0. This gives H_{c1}=4.5 mT in this case.

should be the fourth. Sometimes the third harmonic also shows a signal but this only happens because of mixing with the first harmonic if the first harmonic also has a big signal because of some remnant DC field.

Fig. (5.7) shows an example of the fourth harmonic at 81 K for the detwinned $YBa_2Cu_3O_{6.9}$ sample. This was taken at 81 K and the field modulation amplitude was increased from 0 to 20 mT. The figure only shows the low field section. The two curves show that the signal repeats well whether the sample was zero-field cooled or not to the temperature. The non-zero field cooled data was obtained after similar curves were measured at lower temperatures with field modulation amplitude up to 36 mT. The signal also repeats if we measure while the modulation amplitude is decreasing. This independence on history is probably due to the oscillations which tend to average out any trapped flux.

Fig. (5.7) also shows a sudden upturn at 4.5 mT. Before this the second harmonic is 0. Above it, it's non-zero. This is what we expect upon entering the mixed state so we define that point as H_{c1}. By picking out those points at different temperatures, we can have the temperature dependence of the lower critical field. Fig. (5.8) shows

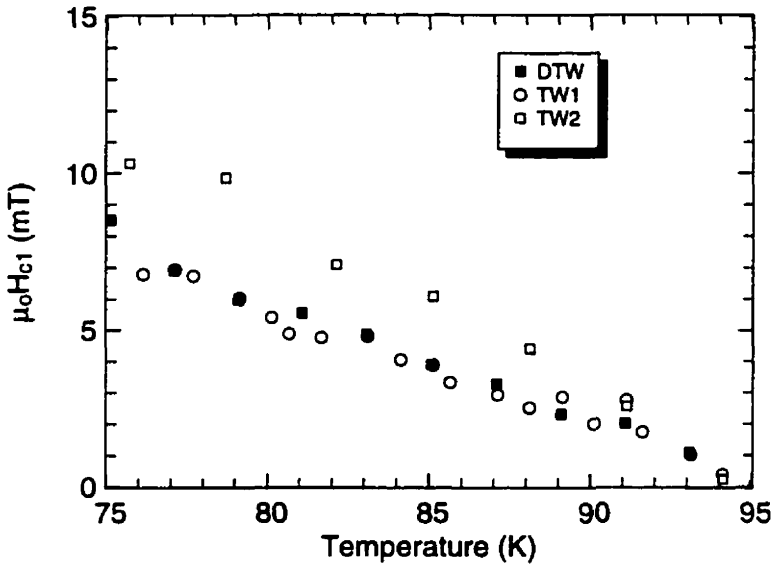

Figure 5.8: Measured H_{c1} above 75K for the three $YBa_2Cu_3O_{6.9}$ samples of table (5.1). The demagnetization and angle have been corrected for.

the locus of those points above 75 K for the three samples of $YBa_2Cu_3O_{6.9}$. Since we do not have a good understanding of the shape of the signal above H_{c1} and that the shape changes at a function of temperature, we pick the points by eye. This can certainly be improved but we have not developed a satisfactory procedure yet. We estimate the relative error of the procedure to be about 10%. Note that the estimated demagnetizing effect as been corrected for. Also, above T_c, the fourth harmonic signal is absolutely 0. Therefore the excitation current going through the piezo does not interact with the field to give a signal. This was expected since the excitation current and the field are small. The critical fields are compatible with the previous measurements mentioned in the previous section.

The critical field below 75 K cannot be extracted reliably. As was the case of the dHvA effect in Sr_2RuO_4 this is because of torque interaction. Here we have

$$\tau = aH^2 \sin(2\theta_o + 2\Delta\theta) \tag{5.11}$$

where a is a constant H is the field modulation amplitude, θ_o is the angle of the orientation of the sample and $\Delta\theta = b\tau$. This b is the same as for the dHvA effect and is the constant that transforms the torque into and angle. For small $\Delta\theta$ this can be

written

$$\tau \approx aH^2\left[(1+2b^2\tau^2)\sin(2\theta_o)+2b\tau\cos(2\theta_o)\right] \tag{5.12}$$

so that keeping only the first order terms

$$\tau = \frac{aH^2\sin(2\theta_o)}{1-aH^2 2b\cos(2\theta_o)} = \frac{\tau_o}{1-\tau_o 2b\cot(2\theta_o)} \approx \tau_o(1+2b\cot(2\theta_o)\tau_o) \tag{5.13}$$

where we write $\tau_o = aH^2\sin(2\theta_o)$, and used the small angle approximation. Hence we have that $\Delta\tau = \tau - \tau_o = 2b\tan(2\theta_o)\tau_o$ so that the relative error is

$$\frac{\Delta\tau}{\tau} = 2b\cot(2\theta_o). \tag{5.14}$$

Therefore the relative error gets worse as you go closer to an axis (0° or 90°). Also the signal gets smaller. But that is where the experiment must be done if we want to measure the critical field along a particular direction. Since we want the H_{c1} of the plane we need to put the field close to the plane. That is the reason of the angles close to 90°. Using $H = H\sin(\omega t)$ in eqn. (5.13) we obtain

$$\tau = \frac{a\sin(2\theta_o)H^2}{2}[1-\cos(2\omega t)] + \frac{a^2\sin(4\theta_o)bH^4}{2}[3-4\cos(2\omega t)+\cos(4\omega t)]. \tag{5.15}$$

So because we have torque interaction we obtain a signal at the fourth harmonic which increases as the fourth power of the amplitude of the modulation field ($a^2 b\sin(4\theta_o)H^4/2$). Fig. (5.9) present data taken at 20 K which shows exactly this behavior. If we express τ in mΩ, then taking $a\sin(2\theta_o) = 80$ mΩ/mT, $b = 8\times10^{-7}$ rad/mΩ^2, $H = 20$ mT and $\theta_o = 80°$ then the amplitude of the fourth harmonic at 20 mT due to the TI should be 2.2×10^3 mΩ. This is bigger than what is measured in fig. (5.9) so TI is certainly a problem.

5.5 *Problems and solutions*

The technique could be promessing if we can avoid the non-linearities. We described in detail the problem due to torque interaction, which is the dominant problem here but there could be other causes. Obviously the cantilever will not remain linear when to large a force is applied on it. The resistivity will tend to saturate and the piezo

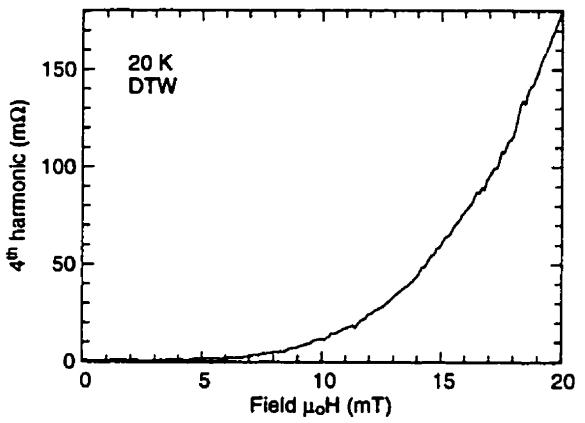

Figure 5.9: Low temperature data showing torque interaction.

will eventually break. Another problem can be due to the electronic. We assume a constant current but it actually varies as the resistance changes. The change in current is first order in changes of resistance but it only brings a second order in $\Delta R/(R_o + 100\ \mathrm{k}\Omega)$ deviation from linearity. At high frequency the effect of the nulling capacitor also gives distortion. This only occurs if the parasitic capacitance is large *i.e.* if the signal without the nulling capacitor is phase shifted by about 45°. In this case, around the nulled condition the signal is linear but as soon as the nulling is not adequate or the signal is large enough the signal starts to shift back into the out of phase component and this rotation of the signal from one phase to another gives the distortion.

The circuit itself, for example the power amplifier for the coil, can be nonlinear. This we have verified to be negligeable for our setup.

A solution to the torque interaction problem and to most of the other possible nonlinearities mentioned above (except the one for the electronics) is to use feedback. This is for the same reason as for the dHvA effect. By using a feedback mechanism to keep the piezo at an almost constant angle, the piezo nonlinearity, the torque interactions, the change in excitation current and the changes in phase due to the parasitic capacitance won't cause any trouble since the resistance will barely change. Of course we will only gain if the feedback mechanism itself is linear. It is more critical in this case than for the dHvA. There even if the feedback mechanism is not

perfectly linear the effect of keeping the angle constant removes the torque interaction. A nonlinearity will only stretch the amplitude of oscillations, it will not make them sawtooth like again. Here we want to use feedback to prevent nonlinearity in the amplitude therefore the feedback should be very linear too if we want to get any improvement. As for the dHvA, the feedback could be achieved by using the sample as one plate of a capacitor. We plan to try this soon.

6

CONCLUSION

In this thesis we presented the first use of a piezoresistive cantilever at milliKelvin temperatures.

We observed an abrupt and hysteretic change of resistance of the device for fields below 10 mT at temperatures below 1 K which we do not understand but we believe it could be due to a weak localization problem. This prevents the use of the device at low fields in this temperature range. At higher fields the magnetoresistance varies smoothly and is not hysteretic.

We used the device to measure the de Haas-van Alphen effect on an organic superconductor, κ-(BEDT-TTF)$_2$Cu(NCS)$_2$, and on Sr_2RuO_4 a compound isostructural to the high-T_c $La_{2-x}Sr_xCuO_4$. For the organic superconductor we observed a frequency of 691 T with an effective mass of 3.64 m_e at an angle of 30° in agreement with previous experiments. We also measured the Dingle temperature to be 0.33 K. This starts increasing when the field is smaller than 4.8 T which is the upper critical field of this material. This increase in scattering due to the superconductivity as been observed before in this material and in others.

We used the dHvA effect as a thermometer to test the effect of high excitation currents through the cantilever on the temperature of the sample. This is important since the sample sits directly on the cantilever and that a high excitation current is needed to have a good sensitivity. To keep the sample as cold as possible we anchored it to the fridge using a copper thermalizing wire attached with silver paint. From the dHvA data we observed that this wire kept the sample cold: with an excitation high enough to bring the cantilever temperature above 1 K the sample only shifted from

100 mK to 150 mK. The observation of dHvA oscillations and the possibility to use a relatively large excitation current, hence to have a good sensitivity, demonstrates that this device can be used at low temperature.

The data obtained from the Sr_2RuO_4 is consistent with a previous experiment. We only observed one of the three Fermi surfaces of this material. The experiment was plagued by a bad thermalization and torque interaction (TI). The TI made the signal sawtooth like instead of sinusoidal. This prevented the accurate calculation of the effective mass and Dingle temperature. The observed frequency was 3.06 kT with a mass of 3.1 m_e and a Dingle temperature of 0.6 K. The TI can be reduced by the use of feedback. The thermalizing problem can probably be solved by using a bigger wire and using a better glue than silver paint. For example, we could use silver epoxy which is used reliably in our group to make contacts on $YBa_2Cu_3O_{6.9}$ for thermalconductivity measurements at low temperature.

We also used the piezo at higher temperatures (4-100 K) and lower fields (less than 40 mT). We used a field modulation technique which improves the sensitivity and removes the problem caused by temperature drifts. Using that technique we can measure accurately the critical temperature of superconductors, as we showed on 1×10^{-3} mm^3 of a $Nb_{0.52}Ti_{0.48}$ wire. We also used the technique to detect the lower critical field, H_{c1}, of a type II superconductor. We measured $YBa_2Cu_3O_{6.9}$ in this way and obtained values consistent with previous experiments. This technique yields H_{c1} directly. The standard techniques require a low field fit and the field at which deviation from this fit occurs yields H_{c1}. Therefore the technique with the piezoresistive cantilever is more straightforward. We must mention that again we encountered a problem of torque interaction. This prevented us from measuring H_{c1} below 75K. The solution here, again, is to use feedback. Hopefully that will enable this device to very simply and rapidly measure H_{c1} in $YBa_2Cu_3O_{6.9}$.

APPENDIX

Here we list all the conversion factors for the piezoresistive cantilevers we used. According to fig. (2.3) and Chapter 2 we use $L = 75\ \mu$m, $c = 75\ \mu$m and $K_A = 20$ N/m. We have that $\Delta z(A) = \frac{5}{2}\Delta z(B)$ and $K_B = \frac{5}{2}K_A = 50$ N/m. Also the cantilever sensitivity is $\Delta R/R_o \Delta z(A) = 0.4$ ppm/Å and we assume $R_o = 2500\ \Omega$.

By using that $\Delta z = F_z/K_A$, $F_z = \tau/L$, and that

$$\theta = \frac{3}{2}\frac{F_z}{K_B L} = \frac{3}{5}\frac{F_z}{K_A L}, \tag{7.1}$$

for small angles, we can extract all the values displayed in table (7.1).

From ↓ to →	θ (rad)	Δz (Å)	$\Delta R/R_o$ (ppm)	ΔR (mΩ)	τ (Nm)	F_z (N)
θ (rad)	1	1.25×10^6	5.0×10^5	1.25×10^6	1.88×10^{-7}	2.5×10^{-3}
Δz (Å)	8.0×10^{-7}	1	0.4	1.0	1.5×10^{-13}	2.0×10^{-9}
$\Delta R/R_o$ (ppm)	2.0×10^{-6}	2.5	1	2.5	3.75×10^{-13}	5.0×10^{-9}
ΔR (mΩ)	8.0×10^{-7}	1.0	0.4	1	1.5×10^{-13}	2.0×10^{-9}
τ (Nm)	5.33×10^6	6.67×10^{12}	2.67×10^{12}	6.67×10^{12}	1	1.33×10^4
F_z (N)	4.0×10^2	5.0×10^8	2.0×10^8	5.0×10^8	7.5×10^{-5}	1

Table 7.1: Table of conversion factors for the piezoresistive cantilevers used in this thesis. To convert for example from τ to θ you take the intersection of the row of the from value (τ) and the column of the to value (θ) and you obtain $\theta = 8 \times 10^{-4}\tau$. Note that the values in mΩ assume $R_o = 2500\ \Omega$, and that the Δz is for the tip (point A of fig. (2.3)). To obtain the displacement at point B multiply by 0.4.

BIBLIOGRAPHY

[1] M. Tortonese, H. Yamada, R. C. Barrett, and C. F. Quate. Atomic force microscopy using a piezoresistive cantilever. In *Proceedings of Transducers '91*, page 448. IEEE, 1991.

[2] D. Zech, J. Hofer, H. Keller, C. Rossel, P. Bauer, and J. Karpinski. Effective mass anisotropy of $HgBa_2Ca_3Cu_4O_{10}$ measured on a microcrystal by means of miniaturized torque magnetometry. *Phys. Rev. B Rapid Communications*, 53(10):R6026–R6029, March 1996.

[3] C. Rossel, P. Bauer, D. Zech, J. Hofer, M. Willemin, and H. Keller. Active microlevers as miniature torque magnetometers. *Journal of Applied Physics*, 79(11):8166–8173, June 1996.

[4] C. W. Yuan, E. Batalla, M. Zacher, A. L. de Lozanne, M. D. Kirk, and M. Tortenese. Low temperature magnetic force microscope utilizing a piezoresistive cantilever. *Applied Physics Letters*, 65(10):1308–1310, 1994.

[5] Hatsumi Urayama, Hideki Yamochi, Gunzi Saito, Kiyokazu Nozawa, Tadashi Sugano, Minoru Kinoshita, Shoichi Sato, Kokichi Oshima, Atsushi Kawamoto, and Jiro Tanaka. A new ambient pressure organic superconductor based on BEDT-TTF with T_c higher than 10 K (T_c =10.4 K. *Chemistry letters*, 1988:55–58, 1988.

[6] Y. Maeno, H. Hashimoto, K. Yoshida, S. Nishizaki, T. Fujita, J. G. Bednorz, and F. Lichtenberg. Superconductivity in a layered perovskite without copper. *Nature*, 372:532–534, December 1994.

[7] A. P. Mackenzie, S. R. Julian, G. G. Lonzarich, Y. Maeno, and T. Fujita. Comment on "extended van Hove singularity in a noncuprate layered superconductor Sr_2RuO_4". *Physical Review Letters*, 78(11):2271–2272, March 1997.

[8] Dror Sarid. *Scanning Force Microscopy: With Applications to Electric, Magnetic, and Atomic Forces.* Oxford University Press, Oxford, revised edition, 1994.

[9] J. S. Brooks, M. J. Naughton, Y. P. Ma, P. M. Chaikin, and R. V. Chamberlin. Small sample magnetometers for simultaneous magnetic and resistive measurements at low temperatures and high magnetic fields. *Review of Scientific Instruments*, 58(1):117–121, January 1987.

[10] D. Zech, C. Rossel, L. Lesne, H. Keller, S. L. Lee, and J. Karpinski. Angle-dependent reversible and irreversible magnetic torque in single-crystalline $Y_2Ba_4Cu_8O_{16}$. *Physical Review B*, 54(17):12535–12542, November 1996.

[11] W. Andraä, H. Bruchlos, T. Eick, R. Hergt, W. Michalke, W. Shüppel, and K. Steenbeck. Critical current density and flux pinning determined by different methods. *Physica C*, 180:184–187, 1991.

[12] W. Andrä, J. Betz, B. Brunner, R. Hergt, H. Lengfellner, K.F. Renk, and K. Steenbeck. Characterization of YBCO films by torque magnetometry. *Physica C*, 180:188–191, 1991.

[13] B. Janossy, H. Gu, R. Cabanel, and L. Fruchter. Anisotropy of the critical current density in bulk $Y_1Ba_2Cu_3O_{7-\delta}$ measured by torque magnetometry for various oxygen deficiencies. *Physica C*, 193:344–352, 1992.

[14] Thomas Albrecht, Marco Tortonese, and Robert Barrett. Piezoresistive cantilever for atomic force microscopy. International patent publication number WO 92/12398, July 1992.

[15] T. F. Rosenbaum, R. F. Milligan, M. A. Paalanen, G. A. Thomas, R. N. Bhatt, and W. Lin. Metal-insulator transition in doped semiconductor. *Physical Review B*, 27(12):7509–7523, June 1983.

[16] Peihua Dai, Youzhu Zhang, and M. P. Sarachik. Magnetoconductance of metallic Si:B near the metal-insulator transition. *Physical Review B*, 46(11):6724–6731, September 1992.

[17] M. Tortonese, R. C. Barrett, and C. F. Quate. Atomic resolution with an atomic force microscope using piezoresistive detection. *Applied Physics Letters*, 62(8):834–836, February 1993.

[18] J. D. Jackson. *Classical Electrodynamics.* John Wiley & Sons, New York, second edition, 1975.

[19] L. D. Landau and E. M. Lifshitz. *Electrodynamics of Continuous Media.* Addison-Wesley Publishing Company, inc., 1960.

[20] Mark W. Zemansky and Richard H. Dittman. *Heat and Thermodynamics.* McGraw-Hill, New York, sixth edition, 1981.

[21] F. Reif. *Fundamentals of Statistical and Thermal Physics.* McGraw-Hill, New York. 1965.

[22] Charles Kittel and Herbert Kroemer. *Thermal Physics.* W. H. Freeman and Company, New York, second edition, 1980.

[23] Adel S. Saada. *Elasticity Theory and Applications.* Krieger Publishing Company, Malabar, Florida, 1993.

[24] Philip M. Morse. *Vibration and Sound.* International Series in Pure and Applied Physics. McGraw-Hill, New York, 1948.

[25] Ray. E. Bolz and George L. Tuve, editors. *CRC Handbook of Tables for Applied Engineering Science.* CRC Press, Cleveland, Oh, second edition, 1973.

[26] F. J. Morin, T. H. Geballe, and C. Herring. Temperature dependence of the piezoresistance of high-purity silicon and germanium. *Physical Review*, 105(2):525–539, January 1957.

[27] M. Tinkham. *Introduction to Superconductivity.* McGraw-Hill, New York, second edition, 1996.

[28] P. G. de Gennes. *Superconductivity of Metals and Alloys.* Addison-Wesley, New York, second edition, 1989.

[29] R. D. Parks, editor. *Superconductivity*, volume 1&2. Marcel Dekker, New York, 1969.

[30] J. Bardeen, L. N. Cooper, and J. R. Schrieffer. Theory of superconductivity. *Physical Review*, 108:1175–1204, 1957.

[31] D. Shoenberg. *Magnetic Oscillations in Metals.* Cambridge Monographs on Physics. Cambridge University Press, Cambridge, 1984.

[32] Y. Onuki, I. Umehara, T. Ebihara, A.K. Albessard, K. Satoh, K. Takita, H. Aoki, S. Uji, and T. Shimizu. de Haas-van Alphen oscillations in the superconducting mixed state of 2H-$NbSe_2$. *Physica B*, 186–188:1050–1052, 1993.

[33] R. Corcoran, P. Meeson, Y. Onuki, P.-A. Probst, M. Springford, K. Takita, H. Harima, G.Y. Guo, and B. L. Byorffy. Quantum oscillations in the mixed state of the type II superconductor 2H-$NbSe_2$. *Journal of Low Temperature Physics*, 6:4479–4492, 1994.

[34] Saša Dukan and Zlatko Tešanović. Superconductivity in a high magnetic field. *Physical Review B*, 49(18):13017–13023, 1994.

[35] M.R. Norman, A.H. MacDonald, and Hiroshi Akera. Magnetic oscillations and quasiparticle band structure in the mixed state of type-II superconductors. *Physical Review B*, 51(9):5927–5942, 1995.

[36] Kazumi Maki. Quantum oscillation in vortex state of type-II superconductors. *Physical Review B*, 44(6):2861–2862, 1991.

[37] Guy Kendall White. *Experimental Techniques in Low-Temperature Physics.* Monographs on the Physics And Chemistry of Materials. Oxford University Press, Oxford, third edition, 1979.

[38] Robert C. Richardson and Eric N. Smith, editors. *Experimental Techniques in Condensed Matter Physics at Low Temperatures.* Frontiers in Physics. Addison-Wesley, Redwood City, CA, 1988.

[39] Frank Pobell. *Matter and Methods at low Temperatures.* Springer-Verlag, Berlin, second edition, 1996.

[40] O. V. Lounasmaa. *Experimental Principles and Methods Below 1K.* Academic Press, London, 1974.

[41] R. C. Weast, editor. *CRC Handbook of Chemistry and Physics.* CRC Press, Florida, 61st edition, 1980.

[42] Paul M. Chaikin and Richard L. Green. Superconducitivity and magnetism in organic metals. *Physics Today*, 39(5):24–32, May 1986.

[43] T. Ishiguro and K. Yamaji. *Organic Superconductors.* Springer-Verlag, Berlin, 1989.

[44] A. M. Kini, U. Geiser, H.H. Wang, K.D. Carlson, J.M. Williams, W.K. Kwok, K.G. Vandervoort, J.E. Thompson, D.L. Stupka, D. Jung, and M.H. Whangbo. A new ambient-pressure organic superconductor, κ-$(ET)_2Cu[N(CN)_2]Br$, with the highest transition temperature yet observed (inductive onset T_c = 11.6 k, resistive onset = 12.5 k). *Inorganic Chemistry*, 29:2555–2557, 1990.

[45] J.M. Williams, A.J. Schultz, U. Geiser, A.M. Carlson, K.d. Kini, H.H. Wang, W.-K. Kwok, M.-H. Whangbo, and J.E. Schirber. Organic superconductors – new benchmarks. *Science*, 252(5012):1501–1508, 1991.

[46] May 1996. CRPS summer school on organic superconductor, Sherbrooke, Qc, Canada.

[47] E. Balthes, D. Schweitzer, I. Heinen, H.J. Keller, W. Stunz, W. Biberacher, A.G.M. Jansen, and E. Steep. Anomalous behavior of magneto-quantum oscillations in the organic supercondcutor κ-(BEDT-TTF)$_2$I$_3$. *Zeitschrift für Physik B*, 99:163–171, 1996.

[48] Kokichi Oshima, Kyouji Araki, Hitoshi Yamazaki, Kiyonori Kato, Yusei Maruyama, Kyuya Yakushi, Takehiko Mori, Hiroo Inokushi, Hatsumi Mori, and Shoji Tanaka. The Fermi surfaces in the κ-type BEDT-TTF based organic superconductors. *Physica C*, 185–189:2689–2690, 1991.

[49] F. A. Meyer, E. Steep, W. Biberacher, P. Christ, A. Lerf, A. G. M. Jansen, W. Joss, P. Wyder, and K. Andres. High-field de Haas-van Alphen studies of κ-(BEDT-TTF)$_2$Cu(NCS)$_2$. *Europhysics Letters*, 32(8):681–686, December 1995.

[50] A.G. Swanson, J.S. Brooks, H. Anzai, N. Konoshita, M. Tokumoto, and K. Murata. Flux jumps, critical fields, and de Hass-van Alpen effect in κ-(BEDT-TTF)$_2$Cu(NCS)$_2$. *Solid State Communications*, 73(5):353–356, 1990.

[51] P.J. van der Wel, J. Caulfield, R. Corcoran, P. Day, S.M. Hayden, W. Hayes, M. Kurmoo, P. Meeson, J. Singleton, and M. Springford. Quantum oscillations near B_{c2} in the organic superconductor κ-(BEDT-TTF)$_2$Cu(NCS)$_2$. *Physica C*, 235–240:2453–2454, 1994.

[52] M. V. Kartsovnik, G. Yu. Logvenov, T. Ishiguro, W. Biberacher, H. Anzai, and N. D. Kushch. Direct observation of the magnetic-breakdown induced quantum interference in the quasi-two-dimensional organic metal (BEDT-TTF)$_2$Cu(NCS)$_2$. *Physical Review Letters*, 77(12):2530–2533, September 1996.

[53] K. Oshima, T. Mori, H. Inokuchi, H. Urayama, H. Yamochi, and G. Saito. Shubnikov-de Haas effect and the Fermi surface in an ambient-pressure organic

superconductor [bis(ethylenedithiolo)tetrathiafulvalene]$_2$Cu(NCS)$_2$. *Phys. Rev. B Rapid Communications*, 38(1):938–941, July 1988.

[54] M. V. Kartsovnik, G. Yu. Logvenov, H. Ito, T. Ishiguro, and G. Saito. Subnikov-de Haas oscillations in the organic superconductor κ-(BEDT-TTF)$_2$Cu[N(CN)$_2$]Br, where BEDT-TTF is bis(ethylenedithio)tetrathiafulvalene. *Phys. Rev. B Rapid Communications*, 52(22):R15715–R15718, December 1995.

[55] V. Vulcanescu, B. Janossy, P. Batail, and L. Fruchter. Magnetization and H_{c2} of a κ-(BEDT-TTF)$_2$Cu[N(CN)$_2$]Br single crystal. *Physical Review B*, 53(5):2590–2593, February 1996.

[56] W. Y. Ching, Yong-Nian Xu, Y. C. Jean, and Y. Lou. Electron states and Fermi surfaces in the organic superconductor κ-(BEDT-TTF)$_2$Cu[N(CN)$_2$]Br. *Physical Review B*, 55(5):2780–2783, February 1997.

[57] Hatsumi Urayama, Hideki Yamochi, Gunzi Saito, Shoichi Sato, Atsushi Kawamoto, Jiro Tanaka, Takehiko Mori, Yusei Maruyama, and Hiroo Inokuchi. Crystal structures of organic superconductor (BEDT-TTF)$_2$Cu(NCS)$_2$, at 298 K and 104 K. *Chemistry letters*, 1988:463–466, 1988.

[58] Yong-Nian Xu, W. Y. Ching, Y. C. Jean, and Y. Lou. First-principles calculation of the electronic and optical properties of the organic superconductor κ-(BEDT-TTF)$_2$Cu(NCS)$_2$. *Physical Review B*, 52(17):12946–12950, November 1995.

[59] John J. Randall and Roland Ward. The preparation of some ternary oxides of the platinum metals. *Journal of the American Chemical Society*, 81:2629–2631, June 1959.

[60] M. Braden, A. H. Moudden, S. Nishizaki, Y. Maeno, and T. Fujita. Structural analysis of Sr_2RuO_4. *Physica C*, 273:248–254, 1997.

[61] S. A. Carter, B. Batlogg, R. J. Cava, J. J. Krajewski, Jr. W. F. Peck, and Jr. L. W. Rupp. Mechanism for the metal-insulator transition in $Sr_2Ir_{1-x}Ru_xO_4$. *Physical Review B*, 51(23):17184–17187, June 1995.

[62] Y. Maeno, S. Nishizaki, K. Yoshida, S. Ikeda, and T. Fujita. Normal-state and superconducting properties of Sr_2RuO_4. *Journal of Low Temperature Physics*, 105(5/6):1577–1586, 1996.

[63] Yoshiteru Maeno, Koji Yoshida, Hiroaki Hashimoto, Shuji Nishizaki, Shin ichi Ikeda, Minoru Nohara, Toshizo Fujita nad Andrwe P. Mackenzie, Nigel E. Hussey, J. Georg Bednorz, and Frank Lichtenberg. Two-dimensional Fermi liquid behavior of the superconductor Sr_2RuO_4. *Journal of the Physical Society of Japan*, 66(5):1405–1408, May 1997.

[64] D.F. Agterberg, T.M. Rice, and M. Sigrist. Orbital dependent superconductivity in Sr_2RuO_4. *Physical Review Letters*, 78(17):3374–3377, April 1997.

[65] Tamio Oguchi. Electronic band structure of the superconductor Sr_2RuO_4. *Phys. Rev. B Rapid Communications*, 51(2):1385–1388, January 1995.

[66] David J. Singh. Relationship of Sr_2RuO_4 to the superconducting layered cuprates. *Physical Review B*, 52(2):1358–1361, July 1995.

[67] G.J. McMullan, M.P. Ray, and R.J. Needs. Comparison of the calculated and observed Fermi surfaces of Sr_2RuO_4. *Physica B*, 223&224:529–531, 1996.

[68] Izumi Hase and Yoshikazu Nishihara. Electronic structure of Sr_2RuO_4 and Sr_2RhO_4. *Journal of the Physical Society of Japan*, 65(12):3957–3963, December 1996.

[69] A. P. Mackenzie, S. R. Julian, A. J. Diver, G. J. McMullan, M. P. Ray, G. G. Lonzarich, Y. Maeno, S. Nishizaki, and T. Fujita. Quantum oscillations in the layered perovskite superconductor Sr_2RuO_4. *Physical Review Letters*, 76(20):3786–3789, May 1996.

[70] A. P. Mackenzie, N. E. Hussey, A. J. Diver, S. R. Julian, Y. Maeno, S. Nishizaki, and T. Fujita. Hall effect in the two-dimensional metal Sr_2RuO_4. *Physical Review B*, 54(10):7425–7429, September 1996.

[71] A.P. Mackenzie, S.R. Julian, A.J. Diver, G.G. Lonzarich N.E. Hussey, Y. Maeno, S. Nishizaki, and T. Fujita. Calculation of thermodynamic and transport properties of Sr_2RuO_4 at low temperatures using known Fermi surface parameter. *Physica C*, 263:510–215, 1996.

[72] T. Yokoya, A. Chainani, T. Takahashi, H. Ding, J. C. Campuzano, H. Katayama-Yoshida, M. Kasai, and Y. Tokura. Angle-resolved photoemission study of Sr_2RuO_4. *Physical Review B*, 54(18):13311–13318, November 1996.

[73] D. H. Lu adn M. Schmidt, T. R. Cummins, S. Shuppler, F. Lichtenberg, and J. G. Bednorz. Fermi surface and extended van Hove singularity in the noncuprate superconductor Sr_2RuO_4. *Physical Review Letters*, 76(25):4845–4848, June 1996.

[74] F. Lichtenberg, A. Catana, J. Mannhart, and D. G. Schlom. Sr_2RuO_4: A metallic substrate for the epitaxial growth of $YBa_2Cu_3O_{7-\delta}$. *Applied Physics Letters*, 60(9):1138–1140, March 1992.

[75] A. Mackenzie, 1997. private communication.

[76] K. Yoshida, Y. Maeno, S. Nishizaki, and T. Fujita. Anisotropic superconductivity of Sr_2RuO_4. *Physica C*, 263:519–522, 1996.

[77] William H. Press, Saul A. Teukolsky, William T. Vetterling, and Brian P. Flannery. *Numerical Recipes in C: the Art of Scientific Computing.* Cambridge University Press, second edition, 1992.

[78] Gerald Burns. *High-Temperature Superconductivity: an Introduction.* Academic Press, 1992.

[79] Physics today, May 1991. Special issue on High temperature superconductors.

[80] Donald M. Ginsberg, editor. *Physical Properties of High Temperature Superconductors*, volume I–V. World Scientific, Singapore, 1989–1996.

[81] Robert Gagnon, Christian Lupien, and Louis Taillefer. T^2 dependence of the resistivity in the Cu-O chains of $YBa_2Cu_3O_{6.9}$. *Physical Review B*, 50(5):3458–3461, August 1994.

[82] Robert Gagnon, Song Pu, Brett Ellman, and Louis Taillefer. Anisotropy of heat conduction in $YBa_2Cu_3O_{6.9}$: A probe of chain superconductivity. *Physical Review Letters*, 78(10):1976–1979, March 1997.

[83] H. Srikanth, B A. Willemsen, T. Jacobs, S. Sridhar, A. Erb, E. Walker, and R. Flükiger. Microwave response of $YBa_2Cu_3O_{6.95}$ crystals: Evidence for a multicomponent order parameter. *Phys. Rev. B Rapid Communications*, 55(22):R14733–R14736, June 1997.

[84] Ruixing Liang, P. Dosanjh, D. A. Bonn, W. N. Hardy, and A. J. Berlinsky. Lower critical fields in an ellipsoid-shaped $YBa_2Cu_3O_{6.95}$ single crystal. *Physical Review B*, 50(6):4212–4215, August 1994.

[85] A. Umezawa, G. W. Crabtree, U. Welp, W. K. Kwok, K. G. Vandervoort, and J. Z. Liu. Twin-boundary effects on flux entry and lower critical fields in single-crystal $YBa_2Cu_3O_{7-\delta}$. *Phys. Rev. B Rapid Communications*, 42(13):8744–8747, November 1990.

[86] E. W. Collings. *A Sourcebook of Titanium Alloy Superconductivity.* Plenum Press, New York, 1983.

IMAGE EVALUATION
TEST TARGET (QA-3)

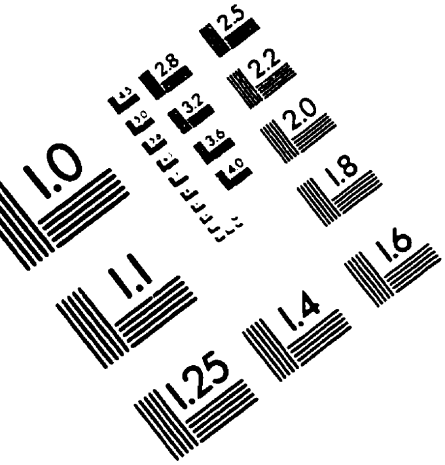

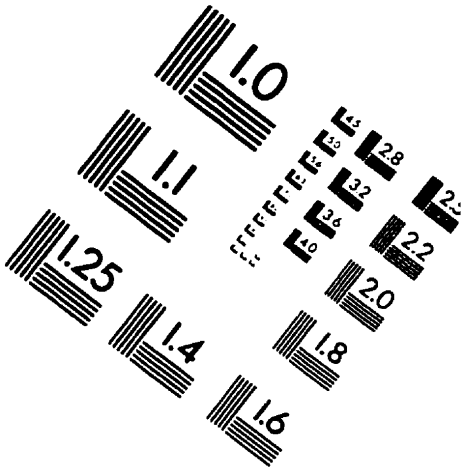

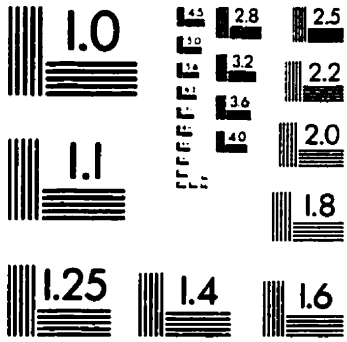

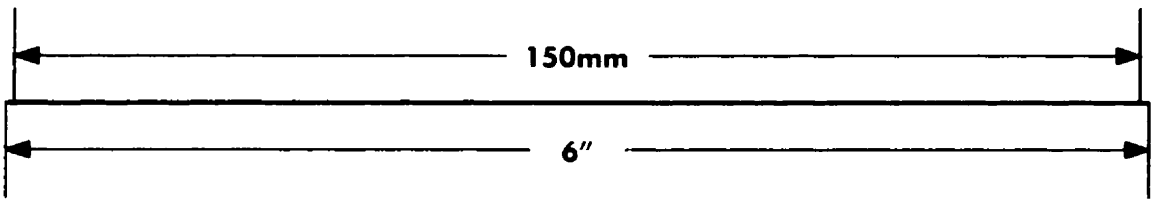

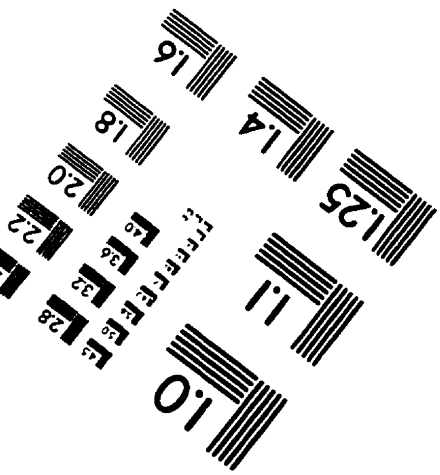

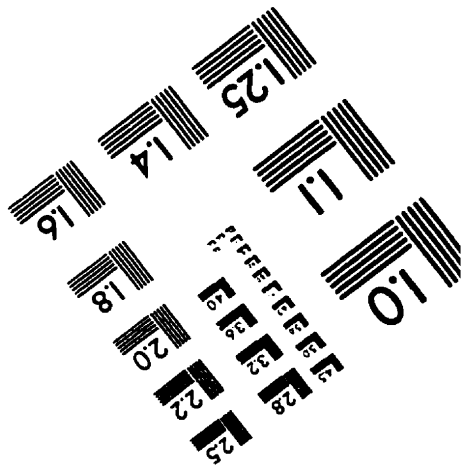

APPLIED IMAGE, Inc
1653 East Main Street
Rochester, NY 14609 USA
Phone: 716/482-0300
Fax: 716/288-5989